

# Topological Spin Textures Enabling Quantum Transmission

Ji Zou,<sup>1</sup> Stefano Bosco,<sup>2</sup> Jelena Klinovaja,<sup>1</sup> and Daniel Loss<sup>1</sup>

<sup>1</sup>*Department of Physics, University of Basel, Klingelbergstrasse 82, 4056 Basel, Switzerland*

<sup>2</sup>*QuTech, Delft University of Technology, Lorentzweg 1, 2628 CJ Delft, The Netherlands*  
(Dated: September 24, 2024)

Quantum spintronics is an emerging field focused on developing novel applications by utilizing the quantum coherence of magnetic systems. Robust information transmission is crucial for achieving fully scalable spintronic devices. However, despite its significance, reliable long-range quantum information transmission in magnetic systems remains a challenging frontier. Here, we introduce a long-distance quantum transmission scheme based on *topological* spin textures in a hybrid system of a magnetic racetrack and spin qubits. We demonstrate this principle by employing the domain wall (DW)—the most fundamental texture—to transport quantum signal between distant qubits. In particular, we propose and analyze an efficient measurement-free protocol that leverages the DW mobility to enable robust entanglement generation between distant qubits. Strikingly, we find that this remote entanglement generation is not only fast and of high fidelity, but also remarkably tunable, capable of being easily turned on and off on-demand by switching the DW initial state. Furthermore, we show that, interestingly, spin qubits can serve as quantum stations for the racetrack, facilitating state transfer among fast-moving DWs on the same track. Our study provides a hybrid quantum platform for scalable quantum computation and opens the door to future explorations of topological textures for quantum information processing in spintronics architectures.

The central theme of quantum spintronics is harnessing quantum coherence of magnetic systems to enable novel functional quantum spintronic devices beyond classical ones [1]. In recent years, significant efforts have been made in the community both theoretically and experimentally [2–18]. These studies have greatly advanced this rapidly emerging field, including the detection of quantum magnonic states [19, 20], their integration with NV centers [21–23] and superconducting qubits [24, 25], and the use of low-dimensional topological textures, such as domain walls (DWs) and skyrmions, as basic units (qubits) for quantum devices [2, 26–28, 30]. However, despite these advancements, a fundamental aspect of practical quantum spintronic devices—the reliable transmission of *quantum* information in magnetic systems—still remains elusive. This capability is crucial and also indispensable for developing fully scalable quantum architectures, akin to traditional spintronics where long-distance signal transport is fundamental to various applications such as racetrack memory [31] and unconventional computation [32]. This has, in fact, also been a critical bottleneck for many other quantum platforms on the path to large-scale devices [33–36], prompting numerous recent efforts across diverse communities to overcome this challenge, such as spin shuttling [37–45] and virtual couplings enabled by cavity photons [46–57], magnons [21, 22, 58–63], Luttinger liquids [64–69], spin chains [70–75] and floating gates [76, 77].

In this work, we propose a robust long-range quantum signal transmission scheme by leveraging nanoscale mobile *topological* spin textures. These magnetic solitons, which naturally exist in magnetic systems, can propagate while preserving their nonlinear structures [78–82]. We consider a hybrid system consisting of distant spin qubits and a magnetic nanowire (racetrack), which hosts topo-

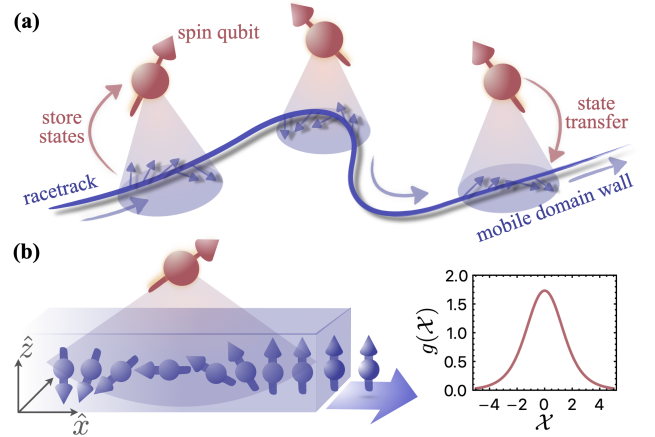


FIG. 1. (a) Schematic diagram illustrating *topological* quantum signal transmission in a hybrid system, where spin qubits interact with a magnetic nanowire (racetrack) hosting mobile DW textures. Spin qubits, acting as quantum stations for the racetrack, can store a quantum state and later transfer it to other topological textures on the same racetrack. (b) A spin qubit interacts with a DW with negative chirality in the magnetic racetrack. The coupling strength profile  $g(\mathcal{X})$  varies as a function of the distance  $\mathcal{X}$  between the qubit and the DW.

logical textures, as depicted in Fig. 1(a). We illustrate the concept by examining magnetic DWs on the track, however, this idea can also be extended to other textures such as skyrmions. Interestingly, by analyzing an explicit remote entanglement protocol, we find that the mobile DW can effectively transport quantum information between distant spin qubits in a highly *controllable* manner over micrometers range. In particular, we show that remote entanglement between spin qubits can be generated by moving the DW at an optimal velocity on the

track, with the ability to turn on and off the process on-demand by adjusting the DW initial state. Remarkably, we also demonstrate that this long-range transmission is not only fast, occurring in the nanosecond regime, but also crucially maintains high fidelity. Furthermore, we reveal that in the hybrid system illustrated in Fig. 1(a), the spin qubits act as effective quantum stations for the DW on the track. These stations enable efficient manipulation of the DW state, such as storing unknown quantum states or coherently transferring states between fast-moving DWs. In the dual picture, DWs serve as mobile stations for spin qubits, enabling distant spin-qubit state transfer. Our findings suggest a new scheme for quantum information transmission using topological textures, marking a crucial step towards the development of fully scalable and functional quantum spintronics devices.

**Model and racetrack-qubit interaction.**— We begin by modeling the effective interaction between spin qubits and the low-energy manifold of the DW in a magnetic wire. Let us consider a quasi-one-dimensional two-sublattice anisotropic ferrimagnetic nanowire, where each unit cell contains two spins, with microscopic Hamiltonian,  $H = J \sum_{\langle i,j \rangle} \mathbf{S}_i \cdot \mathbf{S}_j - \mathcal{K}_z \sum_i (\hat{z} \cdot \mathbf{S}_i)^2 + \mathcal{K}_y \sum_i (\hat{y} \cdot \mathbf{S}_i)^2 - \hbar \sum_i \mathbf{h} \cdot \mathbf{S}_i$ . Here,  $J$  is the antiferromagnetic exchange coupling, whereas  $\mathcal{K}_z$  and  $\mathcal{K}_y$  are both positive-valued, representing the easy- $z$  axis and easy- $xz$  plane anisotropies, respectively. We assume there is a magnetic field  $\mathbf{h} \equiv \gamma \mathbf{B}$  with gyromagnetic ratio  $\gamma$ . This system hosts DW textures described by the continuous vector field  $\mathbf{n}(x)$ , with  $n_x(x) + in_y(x) = e^{i\phi} \text{sech}(x - \mathcal{X})$  and  $n_z(x) = \pm \tanh(x - \mathcal{X})$  [1]. Here,  $\mathcal{X}$  and  $\phi$  represent the spatial position and the azimuthal angle in spin space of the DW. They capture the low-energy DW dynamics. All distances are expressed in units of the DW width  $\lambda \equiv \sqrt{J/\mathcal{K}_z}a$  with lattice spacing  $a$ .

DW textures with  $\phi = 0$  and  $\pi$ , characterized by opposite chiralities,  $\mathcal{C} = (1/\pi) \int_x \hat{y} \cdot (\mathbf{n} \times \partial_x \mathbf{n})$ , are energetically favorable with anisotropies  $\mathcal{K}_z$  and  $\mathcal{K}_y$ . Other energy levels are well-separated from this chirality space (the DW qubit computational space) [2]. Figure 1(b) depicts a profile with  $\mathcal{C} = -1$  (at  $\phi = \pi$ ). Utilizing the collective coordinate quantization technique [2, 26, 84, 85] and integrating out the spatial dynamics, the effective quantum Hamiltonian for a DW moving at a velocity  $v(t)$  can be represented as  $\mathcal{H} = -t_g \tau_x / 2 + \varepsilon(t) \tau_z / 2$  in the chirality space  $\{|\mathcal{C} = \pm 1\rangle\}$ . Here,  $\tau_{x,z}$  are Pauli operators,  $t_g$  is the tunneling rate between the two chirality states, and  $\varepsilon = 2\hbar v(t)/\ell_{so} - 2\pi N \hbar S_e h_x$  is the effective detuning, where  $S_e$  represents the excess spin of the unit cell of the ferrimagnetic nanowire,  $N$  is the amount of unit cells within the DW, and  $\ell_{so}$  is the effective spin-orbit length rooted in the intrinsic spin Berry phase effect of the magnetic system. Explicit expressions for both parameters  $t_g$  and  $\ell_{so}$  are provided in SM [86].

The hybrid quantum system sketched in Fig. 1(a) consists of spin qubits coupled to a racetrack. We assume

the spin qubits are defined within quantum dots in a 2D nonmagnetic layer deposited adjacent to the racetrack, ensuring exchange coupling [59, 87]. Thus the interaction takes the form of  $V = -J_1 \sum_i |\psi(\mathbf{r}_i)|^2 \mathbf{S}_i \cdot \boldsymbol{\sigma}$ , where  $i$  runs over the region of the racetrack beneath the quantum dot,  $J_1$  denotes the exchange interaction strength,  $\psi(\mathbf{r}_i)$  is the orbital part of the quantum dot wavefunction, and  $\boldsymbol{\sigma}$  stands for the spin qubit in the dot. To explore quantum effects, we again employ the collective coordinate quantization, projecting the dynamics onto chirality space. We find the following effective interaction between the spin qubit and the DW low-energy dynamics [86]:

$$\mathcal{V}(t) = -\mathcal{J} g[\mathcal{X}(t)] \tau_z \otimes \sigma_x, \quad (1)$$

where  $\mathcal{J} = J_1 |\psi|^2 N S_e$  is the effective coupling strength and we assumed the wavefunction to be a constant in the dot  $\psi(\mathbf{r}_i) = \psi$  for simplicity. Importantly, the time-dependent coupling envelope function is given by [86]

$$g(\mathcal{X}) = \sum_{k=\pm 1} \arctan[\sinh(l + k\mathcal{X})], \quad (2)$$

which is an even function of  $\mathcal{X}$ , with  $l$  being the radius of the dot.

We stress that the interaction (1) is position-dependent, with  $\mathcal{X}(t)$  representing the time-varying distance between the DW and the center of the quantum dot, while the DW moves on the track. We depict the function  $g(\mathcal{X})$  in Fig. 1(b) for  $l = 1$ , which peaks when the DW is right beneath the dot and exhibits an exponential-decay tail, approaching  $g(\mathcal{X}) \rightarrow (4 \sinh l) \exp\{-|\mathcal{X}(t)|\}$  as the DW moves away. This time-dependent racetrack-spin qubit coupling enables the transport of quantum signals in the hybrid system depicted in Fig. 1(a).

**Entanglement protocol.**— Here we outline and analyze a *measurement-free* remote entanglement protocol based on mobile topological textures. To understand the key idea, we examine a minimal setup involving two spin qubits  $\boldsymbol{\sigma}^{(i)}$  ( $i = 1, 2$ ) coupled to a magnetic racetrack containing a single DW described by  $\boldsymbol{\tau}$  in the low-energy chirality space. The time-dependent system Hamiltonian then takes the following form,

$$\mathcal{H}(t) = - \sum_{i=1,2} \frac{\hbar \omega_s^{(i)}}{2} \sigma_y^{(i)} - \frac{t_g}{2} \tau_x + \frac{\varepsilon(t)}{2} \tau_z - \mathcal{J} \sum_{i=1,2} g[\mathcal{X}_i(t)] \sigma_x^{(i)} \tau_z, \quad (3)$$

where  $\omega_s^{(i)}$  is the spin qubit frequency determined by the magnetic field in the  $y$  direction, and  $\mathcal{X}_i(t)$  stands for the distance between the DW and the spin qubit  $\boldsymbol{\sigma}^{(i)}$ . In our entanglement protocol, (i) starting from trivial initial states, the DW moves beneath the first spin qubit at an optimal velocity  $v_0$  facilitating a  $\sqrt{\text{iSWAP}}$  gate through time-dependent interactions (1). Then, (ii) the DW shuttles from the first to the second qubit, decelerating to a suitable final velocity  $v_f$ , during which the DW

may undergo nontrivial unitary evolution  $U$ . Finally, (iii) the DW approaches and interacts with the second spin qubit, realizing an iSWAP gate. These processes can be represented as the quantum circuit shown in Fig. 2(a). Importantly, this protocol operates without the need for measurements and offers remarkable flexibility to control remote entanglement between distant qubits on-demand by selecting the DW initial state, as discussed below.

To illustrate the key ingredients of the scheme, it is convenient to first rotate the spin axis such that the relevant part of the Hamiltonian in step (i) reads  $\mathcal{H}_1(t) = -\hbar\omega_s^{(1)}\hat{\sigma}_z^{(1)}/2 - t_g\hat{\tau}_z/2 + \mathcal{J}g[\mathcal{X}_1(t)]\hat{\sigma}_x^{(1)}\hat{\tau}_x$ . Here, we omit the second spin qubit, which remains decoupled from both the first spin qubit and the DW in this step. We also assume operation of the DW at the sweet spot  $\varepsilon = 0$  [2] by applying a constant magnetic field  $h_x = v_0/(\pi N S_e \ell_{so})$ . In the interaction picture and in the rotating wave approximation valid at resonance  $t_g = \hbar\omega_s^{(1)}$ , we show that the time-dependent interaction gives rise to the following two-qubit evolution [86]:

$$\mathcal{U} \approx \cos^2 \frac{\Phi}{2} + \sin^2 \frac{\Phi}{2} \hat{\sigma}_z^{(1)} \hat{\tau}_z - \frac{i}{2} \sin \Phi [\hat{\sigma}_x^{(1)} \hat{\tau}_x + \hat{\sigma}_y^{(1)} \hat{\tau}_y], \quad (4)$$

with  $\Phi(v_0) \equiv \frac{\mathcal{J}}{\hbar} \int_0^T g[\mathcal{X}(t)] dt = \frac{6\mathcal{J}}{\hbar v_0}$ .

Here, we assumed that, during this step, the DW moves at a constant velocity,  $\partial_t \mathcal{X}(t) = v_0$ , with  $T$  representing the time required for the DW to traverse the first spin qubit. Importantly, we observe that when the phase factor  $\Phi$  equals  $\pi/4$ , corresponding to  $v_0 = 24\mathcal{J}/(\hbar\pi)$ , the interaction between the qubit and the racetrack leads to an exact DW-spin qubit  $\sqrt{\text{iSWAP}}$  gate. With  $\mathcal{J}/h \approx 100$  MHz ( $h$  is the Planck's constant), the optimal DW velocity is  $v_0 \approx 24$  m/s which is feasible in experiments [88–95]. Consider the initial state of the spin qubit and the DW qubit as  $|\uparrow\rangle_1$  and  $|\downarrow\rangle_{\text{dw}}$ , respectively. Following their interaction, they become entangled, yielding  $(|\uparrow\rangle_1 |\downarrow\rangle_{\text{dw}} - i |\downarrow\rangle_1 |\uparrow\rangle_{\text{dw}})/\sqrt{2}$ .

We now wish to swap the states of the DW and the second spin qubit through their interaction to entangle the two remote qubits. To this end, we reduce the velocity of the DW to extend its interaction time with the second qubit, thereby facilitating the realization of a DW-spin qubit iSWAP gate. To determine the optimal final velocity  $v_f$ , we assume a reduction by  $v_r \equiv v_0 - v_f$ . Consequently, in step (iii), the relevant time-dependent Hamiltonian becomes  $\mathcal{H}_2(t) = -\hbar\omega_s^{(2)}\hat{\sigma}_z^{(2)}/2 - t_g\hat{\tau}_z/2 + (\hbar v_r/\ell_{so})\hat{\tau}_x + \mathcal{J}g[\mathcal{X}_2(t)]\hat{\sigma}_x^{(2)}\hat{\tau}_x$ . This Hamiltonian results in a two-qubit evolution in the interaction picture similar to Eq. (4), but importantly with a different phase factor  $\tilde{\Phi} = 6\mathcal{J} \cos \Theta(v_r)/\hbar v_f$ , with  $\cos \Theta(v_r) = \{1 + [2\hbar v_r/(\ell_{so} t_g)]^2\}^{-1/2}$ . The desired velocity reduction  $v_r$  is determined by

$$\frac{v_0}{v_0 - v_r} = \frac{2}{\cos \Theta(v_r)}, \quad (5)$$

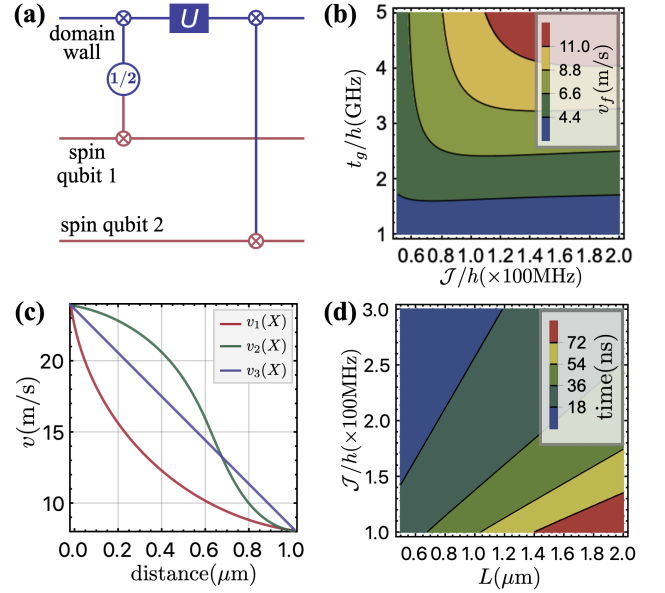


FIG. 2. (a) Quantum circuit representation of the remote entanglement protocol, which is robust to single-qubit rotations, such as  $U$  for the DW, while it moves from the first to the second qubit. (b) Optimal final DW velocity  $v_f$  as a function of the qubit frequency and the racetrack-qubit coupling. (c) Different velocity profiles on the racetrack when reducing the DW velocity from 24 m/s to 8 m/s. (d) Total operational time of the complete entanglement protocol as a function of the coupling and separation between spin qubits.

where the resultant phase factor  $\tilde{\Phi}$  equals  $\pi/2$ , corresponding to an exact iSWAP gate. We remark that the optimal final velocity  $v_f$  is not the naively expected half of the initial velocity, as shown in Fig. 2(b). Instead, it must be smaller than  $v_0/2$ , as the reduction in velocity also reduces the effective coupling,  $\mathcal{J} \rightarrow \mathcal{J} \cos \Theta$ . For a qubit frequency of 3 GHz and  $\mathcal{J}/h \approx 100$  MHz, the optimal final DW velocity is determined to be 8 m/s.

While the DW velocity is reduced during its transition from the first to the second spin qubit in step (ii), it is decoupled from both qubits, with  $g(\mathcal{X}_i) = 0$ , and undergoes a unitary evolution  $U$  governed by the time-dependent Hamiltonian  $\mathcal{H}_{\text{dw}}(t)$ , which depends on the changing velocity profile  $v(\mathcal{X})$  shown in Fig. 2(c). Different velocity profiles lead to different unitary evolutions. However, importantly, our protocol is *robust* to these variations, as the DW remains maximally entangled with the first qubit as it approaches the second qubit. The state, in general, can be represented as  $|\uparrow\rangle_1 |\mathbf{n}\rangle_{\text{dw}} - i |\downarrow\rangle_1 |-\mathbf{n}\rangle_{\text{dw}}$ , with  $\langle \mathbf{n} | -\mathbf{n} \rangle = \langle \downarrow | U^\dagger U | \uparrow \rangle = 0$ . Assuming the second spin qubit is initialized in  $|\uparrow\rangle_2$ , the system state following the local iSWAP gate is described by  $|\Psi_{\text{final}}\rangle \sim \{|\uparrow\rangle_1 |\mathcal{S}^\dagger \mathbf{n}\rangle_2 - i |\downarrow\rangle_1 |-\mathcal{S}^\dagger \mathbf{n}\rangle_2\} \otimes |\uparrow\rangle_{\text{dw}}$ , where  $\mathcal{S} = \text{diag}(1, i)$  is the phase gate. We observe that after step (iii), the two distant spin qubits form a Bell state and leave the DW perfectly disentangled from the system without requiring any projective measurement.

We remark that, instead of varying the DW velocity to change its interaction time with the spin qubits in the entanglement protocol, one may alternatively adjust the effective DW-spin qubit coupling  $\mathcal{J}$  using local electric fields by repositioning the spin qubit relative to the racetrack [33]. This approach allows the realization of a  $\sqrt{\text{iSWAP}}$  gate [ $\Phi = \pi/4$  in Eq. (4)], and subsequently an  $\text{iSWAP}$  gate ( $\Phi = \pi/2$ ) of the hybrid DW-spin qubit, while maintaining a constant DW velocity throughout the entire protocol. Beyond entanglement generation, we *emphasize* that the mobile DW facilitates distant two-qubit gates [86], such as the  $\sqrt{\text{iSWAP}}$  gate, thus enabling universal quantum computing, which is otherwise not possible through methods like sending magnons between distant qubits [59].

A critical parameter of the remote entanglement protocol is the operation time, which comprises three parts: the durations of two local two-qubit gates and the transit time of the DW moving from the first to the second spin qubit. As shown in Fig. 2(d), the total operational time resides in the nanosecond regime for qubit separations on the order of micrometers and coupling strengths in the MHz range. The DW-spin qubit gate time, determined by  $\sim \hbar l/\mathcal{J}$ , is on the order of several nanoseconds for a quantum dot size of 10 nm and  $\mathcal{J}/h \approx 100$  MHz. Meanwhile, the DW transit time spans tens of nanoseconds for a spin qubit separation of approximately  $1 \mu\text{m}$ . Our complete protocol, therefore, operates robustly within the rapid nanosecond regime.

We emphasize that this remote entanglement generation can be interestingly turned on or off on-demand by switching the DW initial state. Specifically, with the initial spin qubits in state  $|\uparrow\rangle_1 |\uparrow\rangle_2$ , flipping the DW initial state from  $|\downarrow\rangle_{\text{dw}}$  to  $|\uparrow\rangle_{\text{dw}}$  changes the outcome from the Bell state to a product state  $|\uparrow\rangle_1 |-\mathcal{S}^\dagger \mathbf{n}\rangle_2$  under exactly the *same* protocol that we described above. Similar entanglement switching can be achieved with other initial states, which are discussed in detail in the SM [86]. Such on-demand control of remote entanglement generation can enable *adaptive* quantum information processing in scalable quantum devices.

**Analysis of fidelity.**—To show the remote entanglement facilitated by the mobile topological textures also have high fidelity  $\mathcal{F}$ , we now focus on both coherent errors resulting from unwanted unitary evolution of the system and incoherent errors caused by noise leading to decoherence. The coupling between the racetrack and the spin qubit leads to the desired two-qubit interaction (1) but also induces a time-dependent magnetic field in the  $z$  direction on the spin qubit,  $h_z[\mathcal{X}(t)] = \mathcal{J} \ln[\cosh(l - \mathcal{X})/\cosh(l + \mathcal{X})]$ . This field causes the spin qubit axis to tilt by a small angle  $\delta\theta \approx 2h_z/\hbar\omega_s$  and induces a small shift in the qubit frequency,  $\delta\omega_s = \sqrt{\omega_s^2 + (2h_z/\hbar)^2} - \omega_s$ .

Importantly, we find that the resultant infidelity of the hybrid DW-spin qubit gate,  $\mathcal{E} = 1 - \mathcal{F}$ , is always bounded

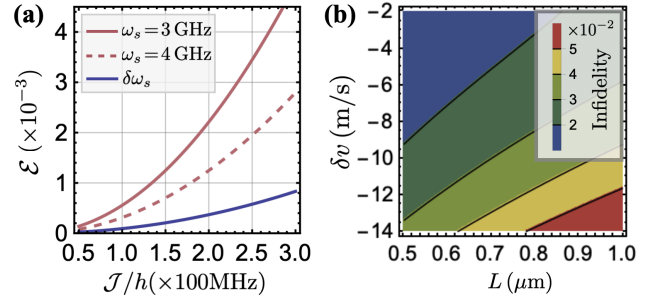


FIG. 3. (a) Two-qubit gate infidelity analysis. The (dashed) red curves illustrate the error caused by spin axis tilting due to an effective field  $h_z$  for different spin qubit frequencies  $\omega_s$ . The purple curve depicts the error induced by qubit frequency shifts. (b) Infidelity due to DW decoherence as a function of the velocity variation and qubit separation.

from above and is analytically given by [86]

$$\mathcal{E} \leq 2 \sin^2 \frac{\delta\theta}{2} + \int_0^T \frac{dt}{2\hbar} \int_0^T \frac{ds}{2\hbar} \tilde{\mathcal{J}}(t) \tilde{\mathcal{J}}(s) \cos[\Phi(t) - \Phi(s)], \quad (6)$$

where  $T$  is again the gate time,  $\Phi(t) = \mathcal{J} \int_0^t g[\mathcal{X}(\tau)] d\tau/\hbar$ , and  $\tilde{\mathcal{J}}(t) = \mathcal{J} g[\mathcal{X}(t)] \sin(\delta\omega_s t)$ . The first term of Eq. (6) represents the maximal infidelity due to the tilting of the spin qubit axis. The (dashed) red curves in Fig. 3(a) show the corresponding value for different spin qubit frequencies  $\omega_s$ , as a function of the coupling  $\mathcal{J}$ , which is on the order of  $10^{-3}$ . The purple curve in Fig. 3(a) illustrates the infidelity induced by the qubit frequency shift, corresponding to the second term in Eq. (6), which is estimated to be on the order of  $10^{-4} \sim 10^{-3}$  for the racetrack-qubit coupling in the MHz regime.

We now focus on the infidelity induced by DW decoherence, as the spin qubit lifetime is an order of magnitude longer than the DW coherence time [33, 96]. With the DW velocity profile  $v(\mathcal{X}) = v_0 + \delta v[\mathcal{X}(t)]$  in general on the racetrack, we show that the resultant infidelity takes the following form [86]:

$$\mathcal{E} \approx \frac{1}{8\hbar^2} \int_{-\infty}^{\infty} \frac{d\omega}{2\pi} S(\omega) |\mathcal{M}(\omega)|^2, \quad \text{with } \mathcal{M} = \int_0^{\bar{T}} d\tau e^{-i\omega\tau} \mathbf{m}(\tau), \quad (7)$$

where  $S(\omega)/\hbar^2 = \alpha N \omega \coth[\hbar\omega/(2k_B T_0)]$  is the noise spectral function with Gilbert damping  $\alpha$  and temperature  $T_0$ ,  $\bar{T}$  is the total operational time, and  $|\mathcal{M}(\omega)|^2$  is the effective filter function with  $\mathbf{m}(t) = (\sin\theta(t) \cos\tilde{\Phi}(t), \sin\theta(t) \sin\tilde{\Phi}(t), \cos\theta(t))$ . Here,  $\theta(t)$  is determined by  $\tan\theta(t) = -t_g \ell_{\text{so}}/[2\hbar\delta v(t)]$  and  $\tilde{\Phi}(t) = \int_0^t d\tau t_g/[\hbar \sin\theta(\tau)]$ . The detailed derivations are presented in SM [86]. Assuming a DW coherence time ( $T_2$ ) of  $0.5 \mu\text{s}$  and a constant  $\delta v$  for simplicity [96], we show the infidelity as a function of  $\delta v$  and the separation  $L$  between qubits in Fig. 3(b). The error is generally on the order of  $10^{-2}$  for a velocity variation  $\delta v \sim -10$  m/s and a qubit separation of micrometers. The remote entangle-

ment generation process, therefore, is not only fast and highly controllable as discussed, but also exceptionally coherent with high fidelity, paving the way for practical quantum spintronic devices for information processing.

**Quantum station for racetrack.**—In the hybrid quantum system depicted in Fig. 1(a), spin qubits also nicely serve as quantum stations for topological spin textures on the racetrack, not only storing but also facilitating the exchange of quantum states, which is crucial for developing a scalable quantum communication system. To this end, we consider a single spin qubit coupled to a racetrack containing multiple DWs. Assuming the quantum station—the spin qubit—is prepared in state  $|\uparrow\rangle_s$ , and DW  $A$  is in a general unknown mixed state  $\rho_A = \sum_i p_i |\psi_i\rangle\langle\psi_i|$ , we propose moving the DW at an optimal velocity  $\tilde{v} = 12\mathcal{J}/(\pi\hbar)$  to store  $\rho_A$  in the spin qubit. This motion facilitates a unitary evolution that precisely executes an iSWAP gate acting on the hybrid DW-spin qubit, culminating in the final state  $\rho_s = \mathcal{S}^\dagger \rho_A \mathcal{S}$  of the spin qubit. By subsequently applying a phase gate, we effectively store the exact unknown state  $\rho_A$  into the spin qubit as shown in Fig. 1(a).

When another DW  $B$  on the racetrack in state  $|\uparrow\rangle_B$  passes by the quantum station at the velocity  $\tilde{v}$  at later time, the time-dependent interaction with the spin qubit again realizes another iSWAP gate, leading to the final state of DW  $B$  as  $\rho_B = \mathcal{S}^\dagger \rho_A \mathcal{S}$ . Therefore, the spin qubit facilitates the transfer of quantum states between fast-moving DWs on the same racetrack, enabling quantum information exchange among different topological spin textures on the same racetrack, which would otherwise be a challenging task. In the dual picture, DWs also act as *mobile* quantum stations for spin qubits, facilitating long-distance spin-qubit state transfer.

We note that by moving the first DW at a slower velocity or adjusting the coupling  $\mathcal{J}$  with local electric fields to enable a hybrid DW-spin qubit  $\sqrt{\text{iSWAP}}$  gate, we can also entangle different DWs on the same track.

**Conclusion.**—We introduced a *reliable* quantum transmission scheme for long distances in a hybrid racetrack-spin qubit system. We illustrated this concept using the simplest topological textures—DWs on the track—to deliver quantum signals between distant spin qubits, akin to a railway system. These mobile topological textures enable controllable, fast, and efficient entanglement generation with high fidelity. Meanwhile, the spin qubits serve as stations, manipulating the topological texture and facilitating communication between different textures on the track. Our study marks a crucial step toward developing fully scalable practical quantum spintronic computing and communication systems.

We thank Banabir Pal and Stuart Parkin for insightful discussions. This work was supported by the Georg H. Endress Foundation and by the Swiss National Science Foundation, NCCR SPIN (grant number 51NF40-180604).

- [1] H. Yuan, Y. Cao, A. Kamra, R. A. Duine, and P. Yan, Quantum magnonics: When magnon spintronics meets quantum information science, *Phys. Rep.* **965**, 1 (2022).
- [2] T. Neuman, D. S. Wang, and P. Narang, Nanomagnonic cavities for strong spin-magnon coupling and magnon-mediated spin-spin interactions, *Physical Review Letters* **125**, 247702 (2020).
- [3] M. Bejarano, F. J. Goncalves, T. Hache, M. Hollenbach, C. Heins, T. Hula, L. Körber, J. Heinze, Y. Berencén, M. Helm, *et al.*, Parametric magnon transduction to spin qubits, *Science Advances* **10**, eadi2042 (2024).
- [4] F. Casola, T. Van Der Sar, and A. Yacoby, Probing condensed matter physics with magnetometry based on nitrogen-vacancy centres in diamond, *Nature Reviews Materials* **3**, 1 (2018).
- [5] I. C. Skogvoll, J. Lidal, J. Danon, and A. Kamra, Tunable anisotropic quantum rabi model via a magnon–spin-qubit ensemble, *Physical Review Applied* **16**, 064008 (2021).
- [6] D. Zhang, X.-M. Wang, T.-F. Li, X.-Q. Luo, W. Wu, F. Nori, and J. You, Cavity quantum electrodynamics with ferromagnetic magnons in a small yttrium-iron-garnet sphere, *npj Quantum Information* **1**, 1 (2015).
- [7] J. Li, S.-Y. Zhu, and G. Agarwal, Magnon-photon-phonon entanglement in cavity magnomechanics, *Physical review letters* **121**, 203601 (2018).
- [8] Y. Li, V. G. Yefremenko, M. Lisovenko, C. Trevillian, T. Polakovic, T. W. Cecil, P. S. Barry, J. Pearson, R. Divan, V. Tyberkevych, *et al.*, Coherent coupling of two remote magnonic resonators mediated by superconducting circuits, *Physical Review Letters* **128**, 047701 (2022).
- [9] T. Van der Sar, F. Casola, R. Walsworth, and A. Yacoby, Nanometre-scale probing of spin waves using single electron spins, *Nature communications* **6**, 7886 (2015).
- [10] P. Andrich, C. F. de las Casas, X. Liu, H. L. Bretscher, J. R. Berman, F. J. Heremans, P. F. Nealey, and D. D. Awschalom, Long-range spin wave mediated control of defect qubits in nanodiamonds, *npj Quantum Information* **3**, 28 (2017).
- [11] M. Dols, S. Sharma, L. Bechara, Y. M. Blanter, M. Kounalakis, and S. V. Kusminskiy, Magnon-mediated quantum gates for superconducting qubits, arXiv preprint arXiv:2406.14967 (2024).
- [12] D. Lachance-Quirion, Y. Tabuchi, S. Ishino, A. Noguchi, T. Ishikawa, R. Yamazaki, and Y. Nakamura, Resolving quanta of collective spin excitations in a millimeter-sized ferromagnet, *Science advances* **3**, e1603150 (2017).
- [13] D. D. Awschalom, C. R. Du, R. He, F. J. Heremans, A. Hoffmann, J. Hou, H. Kurebayashi, Y. Li, L. Liu, V. Novosad, *et al.*, Quantum engineering with hybrid magnonic systems and materials, *IEEE Transactions on Quantum Engineering* **2**, 1 (2021).
- [14] D. Lachance-Quirion, Y. Tabuchi, A. Gloppe, K. Usami, and Y. Nakamura, Hybrid quantum systems based on magnonics, *Applied Physics Express* **12**, 070101 (2019).
- [15] Y. Tserkovnyak, J. Zou, S. K. Kim, and S. Takei, Quantum hydrodynamics of spin winding, *Phys. Rev. B* **102**, 224433 (2020).
- [16] Y. Tserkovnyak and J. Zou, Quantum hydrodynamics of vorticity, *Phys. Rev. Research* **1**, 033071 (2019).
- [17] X.-L. Hei, P.-B. Li, X.-F. Pan, and F. Nori, Enhanced tripartite interactions in spin-magnon-mechanical hybrid

- systems, *Phys. Rev. Lett.* **130**, 073602 (2023).
- [18] Y. Li, W. Zhang, V. Tyberkevych, W.-K. Kwok, A. Hoffmann, and V. Novosad, Hybrid magnonics: Physics, circuits, and applications for coherent information processing, *Journal of Applied Physics* **128** (2020).
- [19] D. Lachance-Quirion, S. P. Wolski, Y. Tabuchi, S. Kono, K. Usami, and Y. Nakamura, Entanglement-based single-shot detection of a single magnon with a superconducting qubit, *Science* **367**, 425 (2020).
- [20] A.-L. E. Römling, A. Vivas-Viaña, C. S. Muñoz, and A. Kamra, Resolving nonclassical magnon composition of a magnetic ground state via a qubit, *Phys. Rev. Lett.* **131**, 143602 (2023).
- [21] M. Fukami, J. C. Marcks, D. R. Candido, L. R. Weiss, B. Soloway, S. E. Sullivan, N. Deegan, F. J. Heremans, M. E. Flatté, and D. D. Awschalom, Magnon-mediated qubit coupling determined via dissipation measurements, *Proceedings of the National Academy of Sciences* **121**, e2313754120 (2024).
- [22] M. Fukami, D. R. Candido, D. D. Awschalom, and M. E. Flatté, Opportunities for long-range magnon-mediated entanglement of spin qubits via on- and off-resonant coupling, *PRX Quantum* **2**, 040314 (2021).
- [23] J. Zou, S. Zhang, and Y. Tserkovnyak, Bell-state generation for spin qubits via dissipative coupling, *Phys. Rev. B* **106**, L180406 (2022).
- [24] Y. Tabuchi, S. Ishino, A. Noguchi, T. Ishikawa, R. Yamazaki, K. Usami, and Y. Nakamura, Coherent coupling between a ferromagnetic magnon and a superconducting qubit, *Science* **349**, 405 (2015).
- [25] M. Kounalakis, G. E. W. Bauer, and Y. M. Blanter, Analog quantum control of magnonic cat states on a chip by a superconducting qubit, *Phys. Rev. Lett.* **129**, 037205 (2022).
- [26] C. Psaroudaki and C. Panagopoulos, Skyrmion qubits: A new class of quantum logic elements based on nanoscale magnetization, *Phys. Rev. Lett.* **127**, 067201 (2021).
- [27] J. Xia, X. Zhang, X. Liu, Y. Zhou, and M. Ezawa, Universal quantum computation based on nanoscale skyrmion helicity qubits in frustrated magnets, *Phys. Rev. Lett.* **130**, 106701 (2023).
- [28] X.-F. Pan, P.-B. Li, X.-L. Hei, X. Zhang, M. Mochizuki, F.-L. Li, and F. Nori, Magnon-skyrmion hybrid quantum systems: Tailoring interactions via magnons, *Phys. Rev. Lett.* **132**, 193601 (2024).
- [29] J. Zou, S. Bosco, B. Pal, S. S. P. Parkin, J. Klinovaja, and D. Loss, Quantum computing on magnetic racetracks with flying domain wall qubits, *Phys. Rev. Res.* **5**, 033166 (2023).
- [30] S. Takei and M. Mohseni, Quantum control of topological defects in magnetic systems, *Phys. Rev. B* **97**, 064401 (2018).
- [31] S. S. Parkin, M. Hayashi, and L. Thomas, Magnetic domain-wall racetrack memory, *Science* **320**, 190 (2008).
- [32] A. V. Chumak, V. I. Vasyuchka, A. A. Serga, and B. Hillebrands, Magnon spintronics, *Nature Physics* **11**, 453 (2015).
- [33] G. Burkard, T. D. Ladd, A. Pan, J. M. Nichol, and J. R. Petta, Semiconductor spin qubits, *Reviews of Modern Physics* **95**, 025003 (2023).
- [34] G. Burkard, M. J. Gullans, X. Mi, and J. R. Petta, Superconductor–semiconductor hybrid-circuit quantum electrodynamics, *Nature Reviews Physics* **2**, 129 (2020).
- [35] A. Blais, A. L. Grimsmo, S. M. Girvin, and A. Wallraff, Circuit quantum electrodynamics, *Reviews of Modern Physics* **93**, 025005 (2021).
- [36] L. Vandersypen, H. Bluhm, J. Clarke, A. Dzurak, R. Ishihara, A. Morello, D. Reilly, L. Schreiber, and M. Veldhorst, Interfacing spin qubits in quantum dots and donors—hot, dense, and coherent, *npj Quantum Information* **3**, 34 (2017).
- [37] T. Fujita, T. A. Baart, C. Reichl, W. Wegscheider, and L. M. K. Vandersypen, Coherent shuttle of electron-spin states, *npj Quantum Information* **3**, 22 (2017).
- [38] A. Mills, D. Zajac, M. Gullans, F. Schupp, T. Hazard, and J. Petta, Shuttling a single charge across a one-dimensional array of silicon quantum dots, *Nature communications* **10**, 1063 (2019).
- [39] J. Yoneda, W. Huang, M. Feng, C. H. Yang, K. W. Chan, T. Tanttu, W. Gilbert, R. Leon, F. Hudson, K. Itoh, *et al.*, Coherent spin qubit transport in silicon, *Nature communications* **12**, 4114 (2021).
- [40] B. Jadot, P.-A. Mortemousque, E. Chanrion, V. Thiney, A. Ludwig, A. D. Wieck, M. Urdampilleta, C. Bäuerle, and T. Meunier, Distant spin entanglement via fast and coherent electron shuttling, *Nature Nanotechnology* **16**, 570 (2021).
- [41] A. Zwerger, S. Amitonov, S. De Snoo, M. Madzik, M. Rimbach-Russ, A. Sammak, G. Scappucci, and L. Vandersypen, Shuttling an electron spin through a silicon quantum dot array, *PRX Quantum* **4**, 030303 (2023).
- [42] A. Noiri, K. Takeda, T. Nakajima, T. Kobayashi, A. Sammak, G. Scappucci, and S. Tarucha, A shuttling-based two-qubit logic gate for linking distant silicon quantum processors, *nature communications* **13**, 5740 (2022).
- [43] I. Seidler, T. Struck, R. Xue, N. Focke, S. Trellenkamp, H. Bluhm, and L. R. Schreiber, Conveyor-mode single-electron shuttling in si/sige for a scalable quantum computing architecture, *npj Quantum Information* **8**, 100 (2022).
- [44] V. Langrock, J. A. Krzywda, N. Focke, I. Seidler, L. R. Schreiber, and L. Cywiński, Blueprint of a scalable spin qubit shuttle device for coherent mid-range qubit transfer in disordered si/sige/sio<sub>2</sub>, *PRX Quantum* **4**, 020305 (2023).
- [45] S. Bosco, J. Zou, and D. Loss, High-fidelity spin qubit shuttling via large spin-orbit interactions, *PRX Quantum* **5**, 020353 (2024).
- [46] X. Mi, M. Benito, S. Putz, D. M. Zajac, J. M. Taylor, G. Burkard, and J. R. Petta, A coherent spin–photon interface in silicon, *Nature* **555**, 599 (2018).
- [47] A. J. Landig, J. V. Koski, P. Scarlino, U. Mendes, A. Blais, C. Reichl, W. Wegscheider, A. Wallraff, K. Ensslin, and T. Ihn, Coherent spin–photon coupling using a resonant exchange qubit, *Nature* **560**, 179 (2018).
- [48] F. Borjans, X. Croot, X. Mi, M. Gullans, and J. Petta, Resonant microwave-mediated interactions between distant electron spins, *Nature* **577**, 195 (2020).
- [49] C. X. Yu, S. Zihlmann, J. C. Abadillo-Uriel, V. P. Michal, N. Rambal, H. Niebojewski, T. Bedecarrats, M. Vinet, É. Dumur, M. Filippone, *et al.*, Strong coupling between a photon and a hole spin in silicon, *Nature Nanotechnology* **18**, 741 (2023).
- [50] P. Harvey-Collard, J. Dijkema, G. Zheng, A. Sammak, G. Scappucci, and L. M. Vandersypen, Coherent spin-spin coupling mediated by virtual microwave photons, *Physical Review X* **12**, 021026 (2022).
- [51] P.-Q. Jin, M. Marthaler, A. Shnirman, and G. Schön,

- Strong coupling of spin qubits to a transmission line resonator, *Physical review letters* **108**, 190506 (2012).
- [52] S. Bosco, P. Scarlino, J. Klinovaja, and D. Loss, Fully tunable longitudinal spin-photon interactions in si and ge quantum dots, *Phys. Rev. Lett.* **129**, 066801 (2022).
- [53] M. Benito, J. R. Petta, and G. Burkard, Optimized cavity-mediated dispersive two-qubit gates between spin qubits, *Physical Review B* **100**, 081412 (2019).
- [54] A. Warren, E. Barnes, and S. E. Economou, Long-distance entangling gates between quantum dot spins mediated by a superconducting resonator, *Physical Review B* **100**, 161303 (2019).
- [55] S. E. Nigg, A. Fuhrer, and D. Loss, Superconducting grid-bus surface code architecture for hole-spin qubits, *Physical review letters* **118**, 147701 (2017).
- [56] M. Trif, V. N. Golovach, and D. Loss, Spin dynamics in inas nanowire quantum dots coupled to a transmission line, *Phys. Rev. B* **77**, 045434 (2008).
- [57] G. Burkard and A. Imamoglu, Ultra-long-distance interaction between spin qubits, *Phys. Rev. B* **74**, 041307 (2006).
- [58] L. Trifunovic, F. L. Pedrocchi, and D. Loss, Long-distance entanglement of spin qubits via ferromagnet, *Phys. Rev. X* **3**, 041023 (2013).
- [59] B. Hetényi, A. Mook, J. Klinovaja, and D. Loss, Long-distance coupling of spin qubits via topological magnons, *Phys. Rev. B* **106**, 235409 (2022).
- [60] J. Zou, S. K. Kim, and Y. Tserkovnyak, Tuning entanglement by squeezing magnons in anisotropic magnets, *Phys. Rev. B* **101**, 014416 (2020).
- [61] B. Flebus and Y. Tserkovnyak, Entangling distant spin qubits via a magnetic domain wall, *Phys. Rev. B* **99**, 140403 (2019).
- [62] W. Xiong, M. Tian, G.-Q. Zhang, and J. Q. You, Strong long-range spin-spin coupling via a kerr magnon interface, *Phys. Rev. B* **105**, 245310 (2022).
- [63] T. c. v. Neuman, D. S. Wang, and P. Narang, Nanomagnonic cavities for strong spin-magnon coupling and magnon-mediated spin-spin interactions, *Phys. Rev. Lett.* **125**, 247702 (2020).
- [64] G. Yang, C.-H. Hsu, P. Stano, J. Klinovaja, and D. Loss, Long-distance entanglement of spin qubits via quantum hall edge states, *Phys. Rev. B* **93**, 075301 (2016).
- [65] T. M. Stace, C. H. W. Barnes, and G. J. Milburn, Mesoscopic one-way channels for quantum state transfer via the quantum hall effect, *Phys. Rev. Lett.* **93**, 126804 (2004).
- [66] J. Viennot, J. Palomo, and T. Kontos, Stamping single wall nanotubes for circuit quantum electrodynamics, *Applied Physics Letters* **104** (2014).
- [67] S. Bosco and D. P. DiVincenzo, Transmission lines and resonators based on quantum hall plasmonics: Electromagnetic field, attenuation, and coupling to qubits, *Phys. Rev. B* **100**, 035416 (2019).
- [68] S. J. Elman, S. D. Bartlett, and A. C. Doherty, Long-range entanglement for spin qubits via quantum hall edge modes, *Phys. Rev. B* **96**, 115407 (2017).
- [69] S. Bosco, D. DiVincenzo, and D. Reilly, Transmission lines and metamaterials based on quantum hall plasmonics, *Phys. Rev. Appl.* **12**, 014030 (2019).
- [70] S. Bose, Quantum communication through an unmodulated spin chain, *Phys. Rev. Lett.* **91**, 207901 (2003).
- [71] M. Friesen, A. Biswas, X. Hu, and D. Lidar, Efficient multiqubit entanglement via a spin bus, *Phys. Rev. Lett.* **98**, 230503 (2007).
- [72] F. K. Malinowski, F. Martins, T. B. Smith, S. D. Bartlett, A. C. Doherty, P. D. Nissen, S. Fallahi, G. C. Gardner, M. J. Manfra, C. M. Marcus, *et al.*, Fast spin exchange across a multielectron mediator, *Nature communications* **10**, 1196 (2019).
- [73] R. Sánchez, G. Granger, L. Gaudreau, A. Kam, M. Pioro-Ladrière, S. A. Studenikin, P. Zawadzki, A. S. Sachrajda, and G. Platero, Long-range spin transfer in triple quantum dots, *Phys. Rev. Lett.* **112**, 176803 (2014).
- [74] T. A. Baart, T. Fujita, C. Reichl, W. Wegscheider, and L. M. K. Vandersypen, Coherent spin-exchange via a quantum mediator, *Nature Nanotechnology* **12**, 26 (2017).
- [75] H. Qiao, Y. P. Kandel, S. Fallahi, G. C. Gardner, M. J. Manfra, X. Hu, and J. M. Nichol, Long-distance superexchange between semiconductor quantum-dot electron spins, *Phys. Rev. Lett.* **126**, 017701 (2021).
- [76] L. Trifunovic, O. Dial, M. Trif, J. R. Wootton, R. Abebe, A. Yacoby, and D. Loss, Long-distance spin-spin coupling via floating gates, *Phys. Rev. X* **2**, 011006 (2012).
- [77] M. Serina, C. Kloeffer, and D. Loss, Long-range interaction between charge and spin qubits in quantum dots, *Phys. Rev. B* **95**, 245422 (2017).
- [78] J. Zang, V. Cros, and A. Hoffmann, eds., *Topology in Magnetism* (Springer International Publishing, 2018).
- [79] J. Zou, S. Zhang, and Y. Tserkovnyak, Topological transport of deconfined hedgehogs in magnets, *Phys. Rev. Lett.* **125**, 267201 (2020).
- [80] X. S. Wang, A. Qaiumzadeh, and A. Brataas, Current-driven dynamics of magnetic hopfions, *Phys. Rev. Lett.* **123**, 147203 (2019).
- [81] Y. Liu, W. Hou, X. Han, and J. Zang, Three-dimensional dynamics of a magnetic hopfion driven by spin transfer torque, *Phys. Rev. Lett.* **124**, 127204 (2020).
- [82] J. Zou, S. K. Kim, and Y. Tserkovnyak, Topological transport of vorticity in heisenberg magnets, *Phys. Rev. B* **99**, 180402 (2019).
- [1] S. K. Kim and O. Tchernyshyov, Mechanics of a ferromagnetic domain wall, *Journal of Physics: Condensed Matter* **35**, 134002 (2023).
- [84] H.-B. Braun and D. Loss, Berry's phase and quantum dynamics of ferromagnetic solitons, *Phys. Rev. B* **53**, 3237 (1996).
- [85] C. Psaroudaki, S. Hoffman, J. Klinovaja, and D. Loss, Quantum dynamics of skyrmions in chiral magnets, *Phys. Rev. X* **7**, 041045 (2017).
- [86] See Supplemental Material for (i) Deriving the effective coupling between spin qubits and domain walls, (ii) Effective unitary evolution under the racetrack-qubit interaction, (iii) Discussion of different initial states and the robustness of the entanglement protocol, (iv) Universality of the distant two-qubit logic, and (v) Detailed derivations of protocol fidelity.
- [87] D. Loss and D. P. DiVincenzo, Quantum computation with quantum dots, *Phys. Rev. A* **57**, 120 (1998).
- [88] O. Gomonay, T. Jungwirth, and J. Sinova, High antiferromagnetic domain wall velocity induced by néel spin-orbit torques, *Phys. Rev. Lett.* **117**, 017202 (2016).
- [89] K.-S. Ryu, L. Thomas, S.-H. Yang, and S. Parkin, Chiral spin torque at magnetic domain walls, *Nature Nanotechnology* **8**, 527 (2013).
- [90] S.-H. Yang, K.-S. Ryu, and S. Parkin, Domain-wall velocities of up to 750 m/s driven by exchange-coupling torque in synthetic antiferromagnets, *Nature Nanotechnology* **10**, 221 (2015).

- [91] K.-J. Kim, S. K. Kim, Y. Hirata, S.-H. Oh, T. Tono, D.-H. Kim, T. Okuno, W. S. Ham, S. Kim, G. Go, Y. Tserkovnyak, A. Tsukamoto, T. Moriyama, K.-J. Lee, and T. Ono, Fast domain wall motion in the vicinity of the angular momentum compensation temperature of ferrimagnets, *Nature Materials* **16**, 1187 (2017).
- [92] S.-H. Yang, R. Naaman, Y. Paltiel, and S. S. P. Parkin, Chiral spintronics, *Nature Reviews Physics* **3**, 328 (2021).
- [93] Y. Guan, X. Zhou, F. Li, T. Ma, S.-H. Yang, and S. S. P. Parkin, Ionitronic manipulation of current-induced domain wall motion in synthetic antiferromagnets, *Nature Communications* **12**, 5002 (2021).
- [94] R. Bläsing, T. Ma, S.-H. Yang, C. Garg, F. K. Dejene, A. T. N'Diaye, G. Chen, K. Liu, and S. S. P. Parkin, Exchange coupling torque in ferrimagnetic co/gd bilayer maximized near angular momentum compensation temperature, *Nature Communications* **9**, 4984 (2018).
- [95] Y. Yoshimura, K.-J. Kim, T. Taniguchi, T. Tono, K. Ueda, R. Hiramatsu, T. Moriyama, K. Yamada, Y. Nakatani, and T. Ono, Soliton-like magnetic domain wall motion induced by the interfacial dzyaloshinskii-moriya interaction, *Nature Physics* **12**, 157 (2016).
- [96] C. Psaroudaki, E. Peraticos, and C. Panagopoulos, Skyrmion qubits: Challenges for future quantum computing applications, *Appl. Phys. Lett.* **123** (2023).



## Supplemental Material for “Topological Spin Textures Enabling Quantum Transmission”

In this Supplemental Material, we present (i) Deriving the effective coupling between spin qubits and domain walls, (ii) Effective unitary evolution under the racetrack-qubit interaction, (iii) Discussion of different initial states and the robustness of the entanglement protocol, (iv) Universality of the distant two-qubit logic, (v) Detailed derivations of protocol fidelity.

### (i) Deriving the effective coupling between spin qubits and domain walls

In this section, we present the derivation of the interaction between spin qubits and domain walls, the Equations (1) and (2) in the main text. We begin with a brief review of the derivation of the domain-wall low-energy dynamics (the construction of the domain-wall chirality qubit Hamiltonian). The microscopic Hamiltonian of the anisotropic ferrimagnetic nanowire is  $H = J \sum_{\langle i,j \rangle} \mathbf{S}_i \cdot \mathbf{S}_j - \mathcal{K}_z \sum_i (\hat{z} \cdot \mathbf{S}_i)^2 + \mathcal{K}_y \sum_i (\hat{y} \cdot \mathbf{S}_i)^2 - \hbar \sum_i \mathbf{h} \cdot \mathbf{S}_i$ , as we presented in the main text. In the construction, we only need to apply a magnetic field in the  $y$  direction, so we assume  $\mathbf{h} = h_y \hat{y}$ . The quantum dynamics of the system can be described as a continuous vector field  $\mathbf{n}(x)$  in the spin path integral formalism. Since our main focus is the domain wall texture, we assume the boundary condition  $n_z(\pm\infty) = \pm\eta$  where  $\eta = \pm 1$ . The domain wall configuration is given by [1]

$$\begin{aligned} n_x(x) &= \cos \phi \operatorname{sech}(x - \mathcal{X}), \\ n_y(x) &= \sin \phi \operatorname{sech}(x - \mathcal{X}), \\ n_z(x) &= \eta \tanh(x - \mathcal{X}), \end{aligned} \quad (\text{S1})$$

Here,  $\mathcal{X}$  and  $\phi$  represent the spatial position and the azimuthal angle in spin space of the DW, as in the main text. All distances are expressed in terms of the DW width  $\lambda \equiv \sqrt{J/\mathcal{K}_z}a$  with lattice spacing  $a$ .

We are particularly interested in the low-energy dynamics of the DW captured by the two soft modes  $\boldsymbol{\psi} \equiv (\mathcal{X}, \phi)$ . Within the collective coordinate approach, the Lagrangian governing such dynamics is given by

$$\mathcal{L}(\boldsymbol{\psi}) = \frac{\mathcal{M}}{2} (\partial_t \boldsymbol{\psi})^2 - \mathcal{A} \cdot \partial_t \boldsymbol{\psi} - \mathcal{F}(\boldsymbol{\psi}), \quad (\text{S2})$$

where the effective mass is  $\mathcal{M} = N\hbar^2/2J$  with  $N$  being the number of unit cells within the DW. The effective gauge field reads  $\mathcal{A} = (\pi\mathcal{M}h_y \cos \phi, 4N\hbar S_e \mathcal{X})/2$ , where  $S_e$  represents the excess spin within the unit cell. We point out that this emergent gauge field arises from the spin Berry phase, accumulated by the net magnetization induced by the applied magnetic field  $h_y$  and by the excess spin. The potential energy is  $\mathcal{F} = 2N\mathcal{K}_y(\sin^2 \phi - 2b_y \sin \phi) + \mathcal{M}\omega_0^2 \mathcal{X}^2/2$ . For clarity,  $b_y$  is defined as the dimensionless magnetic field  $\pi\hbar S_e h_y/4\mathcal{K}_y$ , and we introduced a confining potential characterized by a harmonic length  $\ell_0 = \sqrt{\hbar/(\mathcal{M}\omega_0)}$ . Importantly, the double-well potential for  $\phi$  favoring domain wall textures close to  $\phi = 0$  or  $\pi$ , characterized by opposite chiralities. Note that due to the finite value of  $b_y$ , the favorable profiles are slightly shifted from  $\phi = 0, \pi$ . Both chirality states possess equal energy and are separated by a tunnel barrier,  $\mathcal{V}_0 = 2N\mathcal{K}_y(1 - b_y)^2$  [2].

To examine the low-energy dynamics of the domain wall within the subspace spanned by the two chirality state, we trace out the spatial dynamics and project onto the low-energy sector. This yields the effective description for the domain wall:  $\mathcal{H} = -t_g \tau_x/2$  in the chirality basis  $|\mathcal{C} = \pm 1\rangle$  where  $\tau_x$  is the Pauli matrix and the tunneling splitting reads [2]:

$$t_g \approx 4\hbar\omega_s \sqrt{\frac{2\mathcal{V}_0}{\pi\hbar\omega_s}} \exp\left\{-\left(\frac{4\mathcal{V}_0}{\hbar\omega_s} + \frac{\ell_0}{\ell_{\text{so}}}\right)\right\}. \quad (\text{S3})$$

Here,  $\hbar\omega_s = 2\sqrt{2J\mathcal{K}_y(1 - b_y^2)}$  quantifies the energy gap from the low-energy subspace to the higher energy sector. We define the effective spin-orbital length  $\ell_{\text{so}} \approx (2\hbar/\pi)/(\mathcal{M}h_y + 2N\hbar S_e)$ , which represents the distance the domain wall needs to travel to flip its chirality, an effect driven by the effective gauge field  $\mathcal{A}$ . In the presence of a magnetic field along the racetrack, or when the domain wall is in motion, the two chirality states are no longer equally preferred. This asymmetry introduces a detuning term  $\varepsilon\tau_z/2$  into the Hamiltonian, with  $\varepsilon = 2\hbar v(t)/\ell_{\text{so}} - 8N\mathcal{K}_y b_x$ , where  $v(t)$  represents the velocity of the domain wall on the racetrack. The projection of the  $\phi$  dynamics onto the chirality space can be summarized as  $\cos \phi \rightarrow \gamma_z \tau_z$  and  $\sin \phi \rightarrow \gamma_0 I + \gamma_x \tau_x$ . We work in the same parameter regime as Ref. [2], and we have  $\gamma_z = 0.9, \gamma_0 = 0.14, \gamma_x = 2.7 \times 10^{-3}$ .

To transfer information between the spin qubit and the domain wall qubit, we require a sizable coupling between the spin qubit and the racetrack. To achieve this, we assume that the spin qubits are defined by electrostatic gates in a 2D nonmagnetic layer deposited adjacent to the magnetic racetrack, allowing the spin qubits to be exchange-coupled to the racetrack. We also assume the quantum dot size  $l$  to be around 10 nm in both the  $x$  and  $y$  directions, which is feasible in experiments. The coupling between the spin qubit  $\boldsymbol{\sigma}$  and the spins within the magnetic nanowire is

$$\begin{aligned} V &= -J_1 \sum_{i \in \text{dot}} |\psi(\mathbf{r}_i)|^2 \mathbf{S}_i \cdot \boldsymbol{\sigma} \approx -J_1 |\psi|^2 \sum_{i \in \text{dot}} \mathbf{S}_i \cdot \boldsymbol{\sigma} = -J_1 |\psi|^2 N S_e \int_{-l}^l dx \mathbf{n}(x) \cdot \boldsymbol{\sigma} \\ &= -J_1 |\psi|^2 N S_e \left[ \left( \int_{-l}^l dx n_x(x) \right) \sigma_x + \left( \int_{-l}^l dx n_y(x) \right) \sigma_y + \left( \int_{-l}^l dx n_z(x) \right) \sigma_z \right]. \end{aligned} \quad (\text{S4})$$

Here  $J_1$  is the exchange coupling strength which can be quite large; the summation  $\sum_i$  only runs over the regime in the racetrack covered by the quantum dot;  $|\psi(\mathbf{r}_i)|^2$  is the orbital part of the quantum dot wave function, which we approximate with a constant  $|\psi|^2$  in the dot. We have  $\sum_i |\psi|^2 = 1$ , indicating that  $|\psi|^2$  should be inversely proportional to the quantum dot size. We have again rescaled our coordinate such that we measure the distance in the unit of domain wall width  $\lambda \approx 5$  nm for convenience. For a quantum dot size of 10 nm, we have  $l = 1$  (with  $l$  being radius of the dot).  $N$  and  $S_e$  are the total number of unit cells within the domain wall and the net spin within one unit cell, which we assume to be  $N S_e \sim 1$ . Now we perform the integral and then project  $\phi$  onto the chirality basis. For the  $x$  component, we have

$$\left( \int_{-l}^l dx n_x(x) \right) \sigma_x = \sigma_x \cos \phi \int_{-l}^l dx \operatorname{sech}(x - \mathcal{X}) = g(\mathcal{X}) \sigma_x \cos \phi \rightarrow g(\mathcal{X}) \gamma_z \tau_z \otimes \sigma_x. \quad (\text{S5})$$

Here  $g(\mathcal{X}) = \arctan[\sinh(l + \mathcal{X})] + \arctan[\sinh(l - \mathcal{X})]$ . Similarly for the  $y$  and  $z$  components, we obtain  $\mathcal{J}g(\mathcal{X})(\gamma_0 + \gamma_x \tau_x) \otimes \sigma_y$  and  $h_z(\mathcal{X}) \sigma_z$ , where the effective field due to the racetrack acting on the spin qubit is:

$$h_z(\mathcal{X}) = \eta \mathcal{J} \ln \left[ \frac{\cosh(l - \mathcal{X})}{\cosh(l + \mathcal{X})} \right]. \quad (\text{S6})$$

Here we introduced  $\mathcal{J} = J_1 |\psi|^2 N S_e$  and  $\eta = \pm 1$ , again, stands for the boundary condition of the domain wall texture that introduced in Eq. (S1). We note that  $h_z(\mathcal{X} = 0) = 0$ , indicating that the effect of the racetrack ( $z$  component) averages to zero when the domain wall is right beneath the quantum dot. Then the effective interaction between the spin qubit and the domain wall qubit is given by (involving both  $\boldsymbol{\tau}$  and  $\boldsymbol{\sigma}$ )

$$\mathcal{V}(\mathcal{X}) = -\mathcal{J}g(\mathcal{X}) (\gamma_z \tau_z \otimes \sigma_x + \gamma_x \tau_x \otimes \sigma_y) \approx -\mathcal{J}g(\mathcal{X}) \tau_z \otimes \sigma_x, \quad (\text{S7})$$

which is the Equation (1) in the main text. Here we have approximated  $\gamma_z = 0.9 \approx 1$  and  $\gamma_x \sim 10^{-3} \approx 0$ . We remark that we have dropped single qubit terms, such as the term  $h_z(\mathcal{X}) \sigma_z$ , which will be taken into account later in the analysis of the protocol fidelity.

## (ii) Effective unitary evolution under the racetrack-qubit interaction

In this section, we present the effect of the position-dependent coupling when we move the domain wall across the spin qubit and derive the Eqs. (4) and (5) in the main text. To this end, we consider a single spin qubit coupled to a racetrack with following effective Hamiltonian:

$$\mathcal{H}(t) \approx -\frac{\hbar \omega_s}{2} \sigma_y - \frac{t_g}{2} \tau_x + \frac{\varepsilon(t)}{2} \tau_z - \mathcal{J}g[\mathcal{X}(t)] \sigma_x \otimes \tau_z. \quad (\text{S8})$$

Here, the first term is due to the magnetic field we apply in the  $y$  direction. We have dropped the term  $\mathcal{J}h_z(\mathcal{X}) \sigma_z$  for now, but we will return to it to evaluate the induced coherent error. We note that, though the Hamiltonian above is a  $4 \times 4$  matrix, the dynamics is not exactly solvable due to the nontrivial time-dependent interaction. We will assume the domain wall moves at a constant velocity  $\partial_t \mathcal{X}(t) = v$  during its interaction with the spin qubit.

**Case I: Dynamics with vanishing domain-wall qubit detuning.**— We now work at the sweet spot  $\varepsilon = 0$ , which can be achieved by turning on a small magnetic field in the  $x$  direction. When the domain wall velocity

is  $v = 10$  m/s, the magnetic field is about  $B_x \approx 8$  mT. We first rotate the spin axis:  $\tau_x \rightarrow \hat{\tau}_z, \tau_z \rightarrow -\hat{\tau}_x$  and  $\sigma_y \rightarrow \hat{\sigma}_z, \sigma_z \rightarrow -\hat{\sigma}_y$ . Then the Hamiltonian reads

$$\mathcal{H}(t) = -\frac{\hbar\omega_s}{2}\hat{\sigma}_z - \frac{t_g}{2}\hat{\tau}_z + \mathcal{J}g[\mathcal{X}(t)]\hat{\sigma}_x \otimes \hat{\tau}_x. \quad (\text{S9})$$

We perform the unitary transformation:

$$U_1(t) = \exp\left\{\frac{i\omega_s t}{2}\hat{\sigma}_z\right\} \otimes \exp\left\{\frac{it_g t}{2}\hat{\tau}_z\right\}, \quad \text{and } \mathcal{H} \rightarrow \tilde{\mathcal{H}} = U_1^\dagger \mathcal{H} U_1 + i\hbar\partial_t U_1^\dagger U_1. \quad (\text{S10})$$

In the following, assuming  $t_g = \hbar\omega_s$ , we have

$$\begin{aligned} \tilde{\mathcal{H}}(t) &= \mathcal{J}g[\mathcal{X}(t)]U_1^\dagger \hat{\sigma}_x \otimes \hat{\tau}_x U_1 = \mathcal{J}g[\mathcal{X}(t)] \{ \hat{\sigma}_+ \hat{\tau}_+ \exp[-i(\omega_s + t_g/\hbar)t] + \hat{\sigma}_+ \hat{\tau}_- \exp[i(t_g/\hbar - \omega_s)t] + \text{h.c.} \} \\ &\approx \mathcal{J}g[\mathcal{X}(t)](\hat{\sigma}_+ \otimes \hat{\tau}_- + \hat{\sigma}_- \otimes \hat{\tau}_+) = \frac{\mathcal{J}g[\mathcal{X}(t)]}{2}(\hat{\sigma}_x \otimes \hat{\tau}_x + \hat{\sigma}_y \otimes \hat{\tau}_y), \end{aligned} \quad (\text{S11})$$

where we have used  $t_g = \hbar\omega_s$  and the rotating wave approximation from the first to the second line (which is valid since the coupling strength  $\mathcal{J}$  is in the MHz regime, much smaller than the qubit frequency). Then the evolution due to the Hamiltonian is given by

$$\begin{aligned} \mathcal{U} &= \exp\left\{-\frac{i}{\hbar} \int_0^T d\tau \tilde{\mathcal{H}}(\tau)\right\} = \cos^2 \frac{\Phi}{2} + \sin^2 \frac{\Phi}{2} \hat{\sigma}_z \otimes \hat{\tau}_z - \frac{i}{2} \sin \Phi [\hat{\sigma}_x \otimes \hat{\tau}_x + \hat{\sigma}_y \otimes \hat{\tau}_y] \\ &= \begin{bmatrix} 1 & 0 & 0 & 0 \\ 0 & \cos \Phi & -i \sin \Phi & 0 \\ 0 & -i \sin \Phi & \cos \Phi & 0 \\ 0 & 0 & 0 & 1 \end{bmatrix}, \quad \text{where } \Phi = \frac{\mathcal{J}}{\hbar} \int_0^T d\tau g[\mathcal{X}(\tau)] = \frac{\mathcal{J}}{\hbar v} \int g(\mathcal{X}) d\mathcal{X} \approx \frac{6\mathcal{J}}{\hbar v}, \end{aligned} \quad (\text{S12})$$

where the basis of the matrix is  $|\uparrow\uparrow\rangle, |\uparrow\downarrow\rangle, |\downarrow\uparrow\rangle, |\downarrow\downarrow\rangle$ . Here, we have used the fact that the domain wall moves at a constant velocity  $v$  while it can also be generalized to a time-dependent velocity profile, as long as the motion remains adiabatic with respect to the excited DW states above the two chirality states,  $v \leq 100$  m/s [2]. Here,  $T$  is the time for the domain wall to traverse the spin qubit. This is the Equation (4) in the main text.

**Case II: Dynamics with finite domain-wall qubit detuning.**—With a fixed global magnetic field along the racetrack  $B_x$  in the entanglement protocol, a domain-wall qubit detuning  $\varepsilon \neq 0$  arises when the domain wall moves at a different velocity. We assume the velocity is changed from  $v_0$  to  $v_f$ . In this case, the Hamiltonian takes the form of

$$\mathcal{H}(t) = -\frac{\hbar\omega_s}{2}\hat{\sigma}_z - \frac{t_g}{2}\hat{\tau}_z + \frac{\hbar v_r}{\ell_{\text{so}}}\hat{\tau}_x + \mathcal{J}g[\mathcal{X}(t)]\hat{\sigma}_x \otimes \hat{\tau}_x, \quad (\text{S13})$$

where  $v_r = v_0 - v_f$ . We first rotate the spin space of  $\tau$  in  $xz$ -plane with the rotation matrix:

$$\mathcal{R}(\Theta) = \begin{bmatrix} \cos \Theta & -\sin \Theta \\ \sin \Theta & \cos \Theta \end{bmatrix}, \quad \text{with } \tan \Theta = \frac{2\hbar v_r}{t_g \ell_{\text{so}}}. \quad (\text{S14})$$

We then have the following Hamiltonian:

$$\mathcal{H}(t) = -\frac{\hbar\omega_s}{2}\hat{\sigma}_z - \frac{\Delta}{2}\hat{\tau}_z + \mathcal{J}g[\mathcal{X}(t)]\hat{\sigma}_x \otimes (\cos \Theta \hat{\tau}_x - \sin \Theta \hat{\tau}_z), \quad (\text{S15})$$

where  $\Delta = \sqrt{t_g^2 + (2\hbar v_r/\ell_{\text{so}})^2}$ . We again tune the spin qubit frequency such that they are on resonance  $\hbar\omega_s = \Delta$ . Under the rotating wave approximation in the interaction picture, we have the following Hamiltonian:

$$\tilde{\mathcal{H}}(t) = \frac{\mathcal{J} \cos \Theta g[\mathcal{X}(t)]}{2}(\hat{\sigma}_x \otimes \hat{\tau}_x + \hat{\sigma}_y \otimes \hat{\tau}_y). \quad (\text{S16})$$

We can see two differences compared to Case I: the domain-wall velocity is now  $v_f = v_0 - v_r$ , and the effective coupling changes to  $\mathcal{J} \rightarrow \mathcal{J} \cos \Theta$ .

In the main text, we want the domain wall to initially move at velocity  $v_0$  to achieve a  $\sqrt{\text{iSWAP}}$  gate ( $\Phi = \pi/4$ ), and later at velocity  $v_f$  to realize an iSWAP gate ( $\Phi = \pi/2$ ), which would require:

$$\frac{6\mathcal{J}}{\hbar v_0} = \frac{\pi}{4} \quad \text{and} \quad \frac{6\mathcal{J} \cos \Theta}{\hbar(v_0 - v_r)} = \frac{\pi}{2}, \quad (\text{S17})$$

where we note the angle  $\Theta$  also depends on  $v_r$ . From these two equations, we deduce the Equation (5) in the main text.

## (iii) Discussion of different initial states and the robustness of the entanglement protocol

In this section, we discuss in detail the robustness of the entanglement protocol and present the results for different initial states.

**Case I.**—In the main text, we consider the initial states to be  $|\uparrow\rangle_1 \otimes |\uparrow\rangle_2 \otimes |\downarrow\rangle_{\text{dw}}$ . The entangling gate between the first spin qubit and the domain wall yields the state:

$$|\Psi_1\rangle = \frac{|\uparrow\rangle_1 |\downarrow\rangle_{\text{dw}} - i |\downarrow\rangle_1 |\uparrow\rangle_{\text{dw}}}{2} \otimes |\uparrow\rangle_2. \quad (\text{S18})$$

When the domain wall is moving from the first spin qubit to the second, its velocity is reduced from  $v_0$  to  $v_f$  during which its dynamics is governed by a time-dependent Hamiltonian, leading to a unitary evolution:

$$U = \mathcal{T} \exp \left\{ \int d\tau \mathcal{H}_{\text{dw}}(\tau) \right\}, \quad \text{with } \mathcal{H}_{\text{dw}}(\tau) = -\frac{t_g}{2} \hat{\tau}_z + \frac{\hbar[v_0 - v(\tau)]}{\ell_{\text{so}}} \hat{\tau}_x. \quad (\text{S19})$$

Here,  $\mathcal{T}$  is the time-ordering operator and  $v(\tau)$  is the domain wall velocity at time  $\tau$ . It is clear that the exact evolution depends on how we reduce the velocity  $v(\tau)$  from  $v_0$  to  $v_f$ . Importantly, different evolutions do not change the entanglement between the first spin qubit and the domain wall:

$$|\Psi_1\rangle \rightarrow |\Psi_2\rangle = \frac{|\uparrow\rangle_1 |\mathbf{n}\rangle_{\text{dw}} - i |\downarrow\rangle_1 |-\mathbf{n}\rangle_{\text{dw}}}{2} \otimes |\uparrow\rangle_2, \quad \text{with } |\mathbf{n}\rangle_{\text{dw}} = U |\downarrow\rangle, \text{ and } |-\mathbf{n}\rangle_{\text{dw}} = U |\uparrow\rangle. \quad (\text{S20})$$

This robustness is rooted in the fact that a local unitary transformation does not change the entanglement between two objects. To see the effect of the iSWAP gate, we assume  $|\mathbf{n}\rangle_{\text{dw}} = a |\uparrow\rangle_{\text{dw}} + b |\downarrow\rangle_{\text{dw}}$  and  $|-\mathbf{n}\rangle_{\text{dw}} = b^* |\uparrow\rangle_{\text{dw}} - a^* |\downarrow\rangle_{\text{dw}}$ . Recall that we have  $|\uparrow\downarrow\rangle \rightarrow -i |\downarrow\uparrow\rangle$  and  $|\downarrow\uparrow\rangle \rightarrow -i |\uparrow\downarrow\rangle$  under the iSWAP gate. Then it is clear that, after the iSWAP gate, we have

$$|\mathbf{n}\rangle_{\text{dw}} \otimes |\uparrow\rangle_2 \rightarrow |\uparrow\rangle_{\text{dw}} \otimes |\mathcal{S}^\dagger \mathbf{n}\rangle_2, \quad \text{and } |-\mathbf{n}\rangle_{\text{dw}} \otimes |\uparrow\rangle_2 \rightarrow |\uparrow\rangle_{\text{dw}} \otimes |-\mathcal{S}^\dagger \mathbf{n}\rangle_2, \quad \text{with phase gate } \mathcal{S} = \begin{bmatrix} 1 & 0 \\ 0 & i \end{bmatrix}. \quad (\text{S21})$$

Therefore, with the initial state  $|\uparrow\rangle_1 \otimes |\uparrow\rangle_2 \otimes |\downarrow\rangle_{\text{dw}}$ , the final state is  $\{|\uparrow\rangle_1 |\mathcal{S}^\dagger \mathbf{n}\rangle_2 - i |\downarrow\rangle_1 |-\mathcal{S}^\dagger \mathbf{n}\rangle_2\} \otimes |\uparrow\rangle_{\text{dw}}$ . When we flip the initial state of the domain wall from  $|\downarrow\rangle_{\text{dw}}$  to  $|\uparrow\rangle_{\text{dw}}$ , the first spin qubit will not be entangled with the domain wall under the same protocol. When the domain wall is approaching the second spin qubit, the system state is  $|\uparrow\rangle_1 \otimes |-\mathbf{n}\rangle_{\text{dw}} \otimes |\uparrow\rangle_2$ . Thus, after the iSWAP gate, the final state is  $|\uparrow\rangle_1 \otimes |-\mathcal{S}^\dagger \mathbf{n}\rangle_2 \otimes |\uparrow\rangle_{\text{dw}}$ , which is a trivial product state. We can summarize as

$$|\uparrow\rangle_1 \otimes |\uparrow\rangle_2 \otimes |\downarrow\rangle_{\text{dw}} \rightarrow \frac{|\uparrow\rangle_1 |\mathcal{S}^\dagger \mathbf{n}\rangle_2 - i |\downarrow\rangle_1 |-\mathcal{S}^\dagger \mathbf{n}\rangle_2}{\sqrt{2}} \otimes |\uparrow\rangle_{\text{dw}}, \quad \text{and } |\uparrow\rangle_1 \otimes |\uparrow\rangle_2 \otimes |\uparrow\rangle_{\text{dw}} \rightarrow |\uparrow\rangle_1 \otimes |-\mathcal{S}^\dagger \mathbf{n}\rangle_2 \otimes |\uparrow\rangle_{\text{dw}}. \quad (\text{S22})$$

**Case II.**—We now consider the initial state of the spin qubits to be  $|\uparrow\rangle_1 \otimes |\downarrow\rangle_2$ . To entangle these two qubits, we initialize the domain wall in  $|\downarrow\rangle_{\text{dw}}$ . When the domain wall is approaching the second spin qubit, the state is  $(|\uparrow\rangle_1 |\mathbf{n}\rangle_{\text{dw}} - i |\downarrow\rangle_1 |-\mathbf{n}\rangle_{\text{dw}}) \otimes |\downarrow\rangle_2$ , which evolves into the final entangled state  $(|\uparrow\rangle_1 |\sigma_z \mathcal{S}^\dagger \mathbf{n}\rangle_2 - i |\downarrow\rangle_1 |-\sigma_z \mathcal{S}^\dagger \mathbf{n}\rangle_2) \otimes |\downarrow\rangle_{\text{dw}}$ . On the other hand, when we flip the initial state of the domain wall to  $|\uparrow\rangle_{\text{dw}}$ , the final state is  $|\uparrow\rangle_1 \otimes |-\sigma_z \mathcal{S}^\dagger \mathbf{n}\rangle_2 \otimes |\downarrow\rangle_{\text{dw}}$ . We summarize as

$$|\uparrow\rangle_1 \otimes |\downarrow\rangle_2 \otimes |\downarrow\rangle_{\text{dw}} \rightarrow \frac{|\uparrow\rangle_1 |\sigma_z \mathcal{S}^\dagger \mathbf{n}\rangle_2 - i |\downarrow\rangle_1 |-\sigma_z \mathcal{S}^\dagger \mathbf{n}\rangle_2}{\sqrt{2}} \otimes |\downarrow\rangle_{\text{dw}}, \quad \text{and } |\uparrow\rangle_1 \otimes |\downarrow\rangle_2 \otimes |\uparrow\rangle_{\text{dw}} \rightarrow |\uparrow\rangle_1 \otimes |-\sigma_z \mathcal{S}^\dagger \mathbf{n}\rangle_2 \otimes |\downarrow\rangle_{\text{dw}}. \quad (\text{S23})$$

**Case III.**—We consider the initial state of the spin qubits to be  $|\downarrow\rangle_1 \otimes |\uparrow\rangle_2$ . Following the same procedure, we find that, under the same entanglement protocol, we have

$$|\downarrow\rangle_1 \otimes |\uparrow\rangle_2 \otimes |\uparrow\rangle_{\text{dw}} \rightarrow \frac{|\uparrow\rangle_1 |\mathcal{S}^\dagger \mathbf{n}\rangle_2 + i |\downarrow\rangle_1 |-\mathcal{S}^\dagger \mathbf{n}\rangle_2}{\sqrt{2}} \otimes |\uparrow\rangle_{\text{dw}}, \quad \text{and } |\downarrow\rangle_1 \otimes |\uparrow\rangle_2 \otimes |\downarrow\rangle_{\text{dw}} \rightarrow |\downarrow\rangle_1 \otimes |\mathcal{S}^\dagger \mathbf{n}\rangle_2 \otimes |\uparrow\rangle_{\text{dw}}. \quad (\text{S24})$$

**Case IV.**—Similarly, for the initial state  $|\downarrow\rangle_1 \otimes |\downarrow\rangle_2$ , we have the following map under the exactly the same entanglement protocol:

$$|\downarrow\rangle_1 \otimes |\downarrow\rangle_2 \otimes |\uparrow\rangle_{\text{dw}} \rightarrow \frac{|\uparrow\rangle_1 |\sigma_z \mathcal{S}^\dagger \mathbf{n}\rangle_2 + i |\downarrow\rangle_1 |-\sigma_z \mathcal{S}^\dagger \mathbf{n}\rangle_2}{\sqrt{2}} \otimes |\downarrow\rangle_{\text{dw}}, \quad \text{and } |\downarrow\rangle_1 \otimes |\downarrow\rangle_2 \otimes |\downarrow\rangle_{\text{dw}} \rightarrow |\downarrow\rangle_1 \otimes |\sigma_z \mathcal{S}^\dagger \mathbf{n}\rangle_2 \otimes |\downarrow\rangle_{\text{dw}}. \quad (\text{S25})$$

Therefore, we have demonstrated that the remote entanglement generation process can be turned on and off on demand by switching the DW initial state.

## (iv) Universality of the distant two-qubit logic gate

In this section, we explicitly show that the mobile domain wall facilitates a distant iSWAP gate between two remote spin qubits, and combined with single-qubit rotations, enables universal quantum computation. The quantum circuit representation of such a remote two-qubit gate is shown in Fig. S4. We assume the spin qubit 1 and qubit 2 are initially in states:

$$|\psi\rangle_1 = a|\uparrow\rangle_1 + b|\downarrow\rangle_1, \quad \text{and} \quad |\phi\rangle_2 = c|\uparrow\rangle_2 + d|\downarrow\rangle_2, \quad (\text{S26})$$

where  $a, b, c, d$  are unknown complex numbers in general. We now apply phase gates  $\mathcal{S}$  to these two qubits, resulting in the following states

$$|\tilde{\psi}\rangle_1 = a|\uparrow\rangle_1 + ib|\downarrow\rangle_1, \quad \text{and} \quad |\tilde{\phi}\rangle_2 = c|\uparrow\rangle_2 + id|\downarrow\rangle_2. \quad (\text{S27})$$

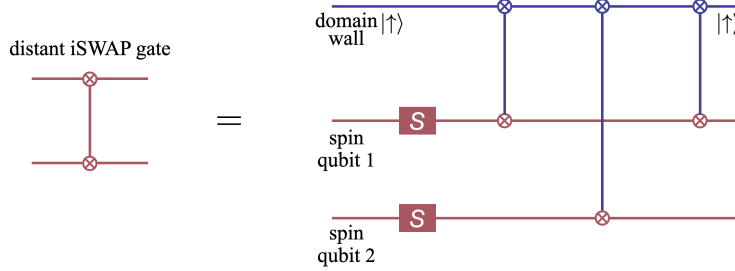


FIG. S4. Quantum circuit representation of a distant iSWAP gate. We first apply the phase gate  $\mathcal{S}$  to the two spin qubits. Next, we move the domain wall (initially in state  $|\uparrow\rangle$ ) across the first spin qubit to realize a local iSWAP gate, then across the second spin qubit to perform another iSWAP. Finally, we move the domain wall back to the first spin qubit, implementing another iSWAP, while disabling the interaction with the second spin qubit on the return path.

We now move the domain wall at a proper velocity (initially in state  $|\uparrow\rangle$ ) across the first spin qubit to realize a local iSWAP gate, which yields

$$|\tilde{\psi}\rangle_1 \otimes |\uparrow\rangle_{\text{dw}} \xrightarrow{\text{iSWAP}} |\uparrow\rangle_1 \otimes (a|\uparrow\rangle_{\text{dw}} + b|\downarrow\rangle_{\text{dw}}). \quad (\text{S28})$$

We continue moving the domain wall across the second spin qubit, leading to another local iSWAP gate:

$$|\tilde{\phi}\rangle_2 \otimes (a|\uparrow\rangle_{\text{dw}} + b|\downarrow\rangle_{\text{dw}}) \xrightarrow{\text{iSWAP}} ac|\uparrow\rangle_2 \otimes |\uparrow\rangle_{\text{dw}} - ibc|\downarrow\rangle_2 \otimes |\uparrow\rangle_{\text{dw}} + ad|\uparrow\rangle_2 \otimes |\downarrow\rangle_{\text{dw}} + idb|\downarrow\rangle_2 \otimes |\downarrow\rangle_{\text{dw}}. \quad (\text{S29})$$

We now move the domain wall back to the first qubit. On its return path, we decouple it from the second spin qubit by shifting the qubit away from the racetrack using a local electric field. As the domain wall passes the first qubit again, it executes another local iSWAP gate:

$$\begin{aligned} & |\uparrow\rangle_1 \otimes [ac|\uparrow\rangle_2 \otimes |\uparrow\rangle_{\text{dw}} - ibc|\downarrow\rangle_2 \otimes |\uparrow\rangle_{\text{dw}} + ad|\uparrow\rangle_2 \otimes |\downarrow\rangle_{\text{dw}} + idb|\downarrow\rangle_2 \otimes |\downarrow\rangle_{\text{dw}}] \\ & \xrightarrow{\text{iSWAP between the first qubit and DW}} |\uparrow\rangle_{\text{dw}} \otimes [ac|\uparrow\rangle_1 |\uparrow\rangle_2 - ibc|\uparrow\rangle_1 |\downarrow\rangle_2 - iad|\downarrow\rangle_1 |\uparrow\rangle_2 + db|\downarrow\rangle_1 |\downarrow\rangle_2]. \end{aligned} \quad (\text{S30})$$

Consequently, the domain wall returns to its initial state  $|\uparrow\rangle_{\text{dw}}$ , fully disentangled from the two spin qubits. Crucially, however, the spin qubit state undergoes a nontrivial evolution:

$$|\text{initial}\rangle = \begin{pmatrix} ac \\ ad \\ bc \\ bd \end{pmatrix} \rightarrow |\text{final}\rangle = \begin{pmatrix} ac \\ -ibc \\ -iad \\ bd \end{pmatrix} = \begin{pmatrix} 1 & & & \\ & 0 & -i & \\ & -i & 0 & \\ & & & 1 \end{pmatrix} |\text{initial}\rangle, \quad (\text{S31})$$

which is equivalent to a remote iSWAP gate acting on the two distant qubits.

We note that the general idea is to first transfer the state of the first spin qubit to the DW, then allow the DW to interact with the second spin qubit to realize an iSWAP gate. Finally, the DW returns to the first spin qubit to transfer its state back to the qubit. This sequence effectively implements the iSWAP gate between the two spin qubits. A similar approach can be applied to realize a  $\sqrt{\text{iSWAP}}$  gate. Instead of performing an iSWAP gate in the second step, we can implement a  $\sqrt{\text{iSWAP}}$  gate between the second spin qubit and the DW. Then, this process would ultimately result in a  $\sqrt{\text{iSWAP}}$  gate between the distant qubits.

## (v) Detailed derivations of protocol fidelity

In this section, we present a detailed analysis of the fidelity of the entanglement protocol and derive Equations (6) and (7) in the main text. We consider both coherent and incoherent errors. Calculating the fidelity of a quantum operation is essential to evaluate how closely a real operation  $\mathcal{U}_R$  matches an ideal one  $\mathcal{U}_T$ , which can be represented as

$$\mathcal{F} = \frac{1}{\dim[\mathcal{U}]} \text{Tr} [\mathcal{U}_R \mathcal{U}_T^\dagger]. \quad (\text{S32})$$

**Coherent errors.**—In our previous analysis, we have dropped the effective magnetic field  $h_z(\mathcal{X})$  acting on the spin qubit due to its coupling to the racetrack. Taking this term into account, the total Hamiltonian describing the interaction between spin qubit and domain wall qubit is given by

$$\begin{aligned} \mathcal{H}(t) &= -\frac{\hbar\omega_s}{2}\sigma_y - h_z[\mathcal{X}(t)]\sigma_z - \frac{t_g}{2}\tau_x - \mathcal{J}g[\mathcal{X}(t)]\sigma_x \otimes \tau_z \\ &= -\frac{\hbar\omega_s}{2}\hat{\sigma}_z + h_z[\mathcal{X}(t)]\hat{\sigma}_y - \frac{t_g}{2}\hat{\tau}_z + \mathcal{J}g[\mathcal{X}(t)]\hat{\sigma}_x \otimes \hat{\tau}_x, \end{aligned} \quad (\text{S33})$$

where we again rotate the spin axis for convenience. We now conduct a time-dependent spin rotation around  $x$  axis in the spin space:

$$U[\theta(t)] = \exp\left\{i\left[\theta(t) - \frac{\pi}{2}\right]\frac{\hat{\sigma}_x}{2}\right\}, \quad \text{with} \quad \cos\theta(t) = \frac{2h_z(t)/\hbar}{\sqrt{\omega_s^2 + (2h_z/\hbar)^2}} \rightarrow \theta(t) \approx \frac{\pi}{2} - \frac{2h_z(t)}{\hbar\omega_s}, \quad (\text{S34})$$

where we have used the fact that the induced effective magnetic field is one order of magnitude smaller than the qubit frequency  $h_z \sim \mathcal{J} \ll \hbar\omega_s$ . We note that the spin axis is tilted by a small angle  $2h_z(t)/\hbar\omega_s$  due to this effective magnetic field. Then the Hamiltonian is given by:

$$\begin{aligned} \mathcal{H}_R &= U^\dagger[\theta(t)]HU[\theta(t)] + i\hbar(\partial_t U^\dagger[\theta(t)])U[\theta(t)] = -\frac{\hbar\sqrt{\omega_s^2 + [2h_z(t)/\hbar]^2}}{2}\hat{\sigma}_z + \frac{\hbar\dot{\theta}(t)}{2}\hat{\sigma}_x - \frac{t_g}{2}\hat{\tau}_z + \mathcal{J}(t)\hat{\sigma}_x \otimes \hat{\tau}_x \\ &\approx -\frac{\hbar\omega_s}{2}\hat{\sigma}_z - \frac{t_g}{2}\hat{\tau}_z + \mathcal{J}(t)\hat{\sigma}_x \otimes \hat{\tau}_x. \end{aligned} \quad (\text{S35})$$

Here, we have neglected two terms. The first term is the qubit frequency renormalization due to the effective magnetic field,  $\delta\omega_s = \sqrt{\omega_s^2 + (2h_z/\hbar)^2} - \omega_s$ . We will return to this frequency shift later. The second term we dropped is rooted in the time dependence of the tilting angle  $\dot{\theta}(t) \approx \Delta\theta/T_g \sim 2\pi \times 2$  MHz, where  $\Delta\theta \sim 0.03$  and  $T_g \sim 2$  ns is the local two-qubit gate time. The error induced by this term would be negligible compared to the error that we are considering here induced by the effective magnetic field, which is on the order of 100 MHz. Thus, we will neglect this term in the following analysis.

We now switch to the interaction picture by the unitary transformation  $\mathcal{U}(t) = \exp\{i\omega_s t(\hat{\sigma}_z + \hat{\tau}_z)/2\}$ . Under the rotating wave approximation and working at  $t_g = \hbar\omega_s$ , we arrive at the Hamiltonian  $H_I(t) \approx \mathcal{J}[g(t)/2](\hat{\sigma}_x \otimes \hat{\tau}_x + \hat{\sigma}_y \otimes \hat{\tau}_y)$ . Thus, the real operation in the original frame is given by

$$\mathcal{U}_R = U[\theta(T_g)]\mathcal{U}(T_g) \exp\left\{-\frac{i}{\hbar} \int_0^{T_g} d\tau H_I(\tau)\right\} \mathcal{U}^\dagger(0)U^\dagger[\theta(0)]. \quad (\text{S36})$$

On the other hand, the target (ideal) evolution is given by

$$\mathcal{U}_T = \mathcal{U}(T_g) \exp\left\{-\frac{i}{\hbar} \int_0^{T_g} d\tau H_I(\tau)\right\} \mathcal{U}^\dagger(0), \quad (\text{S37})$$

where  $T_g$  is the gate operational time. Utilizing Eq. (S32), we obtain the fidelity

$$\mathcal{F} = \cos^2 \frac{\delta\theta}{2} - \cos\Phi \cos(\omega_s T_g) \sin^2 \frac{\delta\theta}{2}. \quad (\text{S38})$$

Here,  $\Phi = [\mathcal{J}/(\hbar v)] \int g(\mathcal{X})d\mathcal{X} \approx 6\mathcal{J}/(\hbar v)$  and  $\delta\theta$  is the maximal tilting angle of the spin axis due to the effective magnetic field  $h_z$ , where we can approximate it as  $\delta\theta \sim \mathcal{J}/\hbar\omega_s$ . Then the error induced by this spin axis tilting is

$$1 - \mathcal{F} = \sin^2 \frac{\delta\theta}{2} + \cos\Phi \cos(\omega_s T_g) \sin^2 \frac{\delta\theta}{2} \leq 2 \sin^2 \frac{\delta\theta}{2}. \quad (\text{S39})$$

In the discussion above, we have pointed out that the effective magnetic field also shifts the qubit frequency. Besides, in experiments, it may also be difficult to make the two qubits exactly on resonance  $\hbar\omega_s = t_g$ . So here we investigate the two-qubit gate error induced by a detuning between the two frequencies. We consider the following Hamiltonian:

$$\mathcal{H}(t) = -\frac{\hbar(\omega_s + \delta\omega_s)}{2}\hat{\sigma}_z - \frac{\hbar\omega_s}{2}\hat{\tau}_z + \mathcal{J}g(t)\hat{\sigma}_x \otimes \hat{\tau}_x. \quad (\text{S40})$$

We again move to the interaction picture and apply the rotating wave approximation, yielding

$$\mathcal{H}_I(t) \approx \mathcal{J}g(t) [\hat{\sigma}_+ \hat{\tau}_- e^{-i\delta\omega_s t} + \text{h.c.}] = \frac{\mathcal{J}g(t) \cos(\delta\omega_s t)}{2}(\hat{\sigma}_x \hat{\tau}_x + \hat{\sigma}_y \hat{\tau}_y) - \frac{\mathcal{J}g(t) \sin(\delta\omega_s t)}{2}(\hat{\sigma}_x \hat{\tau}_y - \hat{\sigma}_y \hat{\tau}_x). \quad (\text{S41})$$

For simplicity, we consider  $\delta\omega_s$  to be on the order of 20 MHz or less (the frequency shift due to the effective magnetic field  $h_z$  is about 2 MHz), which implies  $\delta\omega_s T_g \ll 1$ . We then approximate the Hamiltonian with

$$\mathcal{H}_I(t) \approx \frac{\mathcal{J}g(t)}{2}(\hat{\sigma}_x \hat{\tau}_x + \hat{\sigma}_y \hat{\tau}_y) - \frac{\mathcal{J}g(t) \sin(\delta\omega_s t)}{2}(\hat{\sigma}_x \hat{\tau}_y - \hat{\sigma}_y \hat{\tau}_x). \quad (\text{S42})$$

To see the effect of the last term due to finite  $\delta\omega_s$ , we apply the unitary transformation

$$\mathcal{U}_2(t) = \exp\left\{-\frac{i}{2}\Phi(t)(\hat{\sigma}_x \hat{\tau}_x + \hat{\sigma}_y \hat{\tau}_y)\right\}, \quad \text{with } \Phi(t) = (\mathcal{J}/\hbar) \int_0^t g(\tau) d\tau, \quad (\text{S43})$$

which leads to the following Hamiltonian

$$\mathcal{H}_2(t) = -\frac{\mathcal{J}g(t) \sin(\delta\omega_s t)}{2}\mathcal{U}_2^\dagger(t)(\hat{\sigma}_x \hat{\tau}_y - \hat{\sigma}_y \hat{\tau}_x)\mathcal{U}_2(t) = -\frac{\mathcal{J}g(t) \sin(\delta\omega_s t)}{2}[\cos \Phi(t)(\hat{\sigma}_x \hat{\tau}_y - \hat{\sigma}_y \hat{\tau}_x) + \sin \Phi(t)(\hat{\sigma}_z - \hat{\tau}_z)]. \quad (\text{S44})$$

Then the fidelity is given by

$$\mathcal{F} = \frac{1}{4} \text{Tr } \mathcal{T} \exp\left\{-\frac{i}{\hbar} \int_0^{T_g} d\tau \mathcal{H}_2(\tau)\right\} \approx 1 - \left[\int_0^{T_g} d\tau \frac{\mathcal{J}g(\tau) \sin(\delta\omega_s \tau) \cos \Phi(\tau)}{2\hbar}\right]^2 - \left[\int_0^{T_g} d\tau \frac{\mathcal{J}g(\tau) \sin(\delta\omega_s \tau) \sin \Phi(\tau)}{2\hbar}\right]^2. \quad (\text{S45})$$

Thus the corresponding error is

$$\begin{aligned} 1 - \mathcal{F} &= \left[\int_0^{T_g} d\tau \frac{\mathcal{J}g(\tau) \sin(\delta\omega_s \tau) \cos \Phi(\tau)}{2\hbar}\right]^2 + \left[\int_0^{T_g} d\tau \frac{\mathcal{J}g(\tau) \sin(\delta\omega_s \tau) \sin \Phi(\tau)}{2\hbar}\right]^2 \\ &= \frac{\mathcal{J}^2}{4\hbar^2} \int_0^{T_g} d\tau \int_0^{T_g} ds g(\tau)g(s) \sin(\delta\omega_s \tau) \sin(\delta\omega_s s) [\cos \Phi(\tau) \cos \Phi(s) + \sin \Phi(\tau) \sin \Phi(s)] \\ &= \int_0^{T_g} \frac{dt}{2\hbar} \int_0^{T_g} \frac{ds}{2\hbar} \check{\mathcal{J}}(t)\check{\mathcal{J}}(s) \cos[\Phi(t) - \Phi(s)], \quad \text{with } \check{\mathcal{J}}(t) = \mathcal{J}g(t) \sin(\delta\omega_s t). \end{aligned} \quad (\text{S46})$$

Combing with Eq. (S39), we have derived the Equation (6) in the main text.

**Error due to noise.**—Here we discuss the error induced by the noise in the system. We note that while the spin qubits can reach decoherence times of up to  $10\mu\text{s}$  in experiments, the domain wall qubit lifetime is estimated to be of submicrosecond ( $\sim 0.5\mu\text{s}$ ) with feasible experimental parameters in current materials. Consequently, the fidelity of our system is primarily limited by the noise affecting the domain wall qubit. The dominant fluctuating term in the domain wall qubit Hamiltonian arises from the fluctuations of the azimuthal angle of the domain wall texture in spin space, represented as  $\delta H = [h(t)/2]\tau_z$ . Here,  $h(t)$  is the fluctuating field, characterized by the classical ensemble average and their correlation function:  $\langle h(t) \rangle = 0$  and  $\langle h(t)h(s) \rangle = S(t-s)$ , where  $S(t)$  is related to the dissipation parameter via the fluctuation dissipation theorem and the corresponding spectral function is  $S(\omega) = \hbar^2 \alpha N \omega \coth[\hbar\omega/(2k_B T_0)]$ . Here  $\alpha$  is Gilbert damping and  $T_0$  is the temperature. Let us write down the Hamiltonian for the domain wall:

$$\mathcal{H}(t) = -\frac{t_g}{2}\hat{\tau}_z - \frac{\hbar\delta v[\mathcal{X}(t)]}{\ell_{\text{so}}}\hat{\tau}_x + \frac{h(t)}{2}\hat{\tau}_x, \quad (\text{S47})$$

where we consider the domain wall velocity profile on the racetrack to be  $v(\mathcal{X}) = v_0 + \delta v[\mathcal{X}(t)]$  and we also have rotated the spin axis. We again rotate the spin axis such that

$$\mathcal{H}(t) = -\frac{\hbar\Omega(t)}{2}\hat{\tau}_z + \frac{h(t)}{2}\{\sin[\theta(t)]\hat{\tau}_x - \cos[\theta(t)]\hat{\tau}_z\}, \quad \text{with } \frac{\hbar\Omega(t)}{2} = \sqrt{(t_g/2)^2 + [\hbar\delta v(t)/\ell_{\text{so}}]^2} \quad \text{and } \tan \theta(t) = -\frac{t_g \ell_{\text{so}}}{2\hbar\delta v(t)}. \quad (\text{S48})$$

We now apply the following unitary transformation:

$$\mathcal{U}_1 = \exp\left\{i\frac{\tilde{\Phi}(t)}{2}\hat{\tau}_z\right\}, \quad \text{with } \tilde{\Phi}(t) = \int_0^t d\tau \Omega(\tau), \quad (\text{S49})$$

which yields

$$\mathcal{H}_1(t) = \frac{h(t)}{2} \sin\theta(t) \left[ \cos\tilde{\Phi}(t)\hat{\tau}_x + \sin\tilde{\Phi}(t)\hat{\tau}_y \right] - \frac{h(t)}{2} \cos\theta(t) \hat{\tau}_z. \quad (\text{S50})$$

The fidelity therefore is given by

$$\begin{aligned} \mathcal{F} &= \text{Tr } \mathcal{T} \exp\left\{-\frac{i}{\hbar} \int_0^T d\tau \mathcal{H}_1(\tau)\right\} = 1 - \frac{1}{2\hbar^2} \int_0^T d\tau \int_0^T d\tau' \text{Tr} [\mathcal{H}_1(\tau)\mathcal{H}_1(\tau')] \\ &= 1 - \frac{1}{8\hbar^2} \int_0^T d\tau \int_0^T d\tau' h(\tau)h(\tau') \sin\theta(\tau) \sin\theta(\tau') \cos[\tilde{\Phi}(\tau) - \tilde{\Phi}(\tau')] - \frac{1}{8\hbar^2} \int_0^T d\tau \int_0^T d\tau' h(\tau)h(\tau') \cos\theta(\tau) \cos\theta(\tau') \\ &= 1 - \frac{1}{8\hbar^2} \int_{-\infty}^{\infty} \frac{d\omega}{2\pi} S(\omega) F(\omega, T), \end{aligned} \quad (\text{S51})$$

where  $T$  is the total shuttling time of the domain wall and  $F(\omega, T)$  is the effective filter function determined by:

$$F(\omega, T) = \left| \int_0^T d\tau e^{-i\omega\tau} \sin\theta(\tau) \cos\tilde{\Phi}(\tau) \right|^2 + \left| \int_0^T d\tau e^{-i\omega\tau} \sin\theta(\tau) \sin\tilde{\Phi}(\tau) \right|^2 + \left| \int_0^T d\tau e^{-i\omega\tau} \cos\theta(\tau) \right|^2. \quad (\text{S52})$$

For convenience, we can introduce a time-dependent vector:

$$\mathbf{m}(\tau) = [\sin\theta(\tau) \cos\tilde{\Phi}(\tau), \sin\theta(\tau) \sin\tilde{\Phi}(\tau), \cos\theta(\tau)]. \quad (\text{S53})$$

The filter function then can be written in the following compact form:

$$F(\omega, T) = |\mathcal{M}(\omega, T)|^2, \quad \text{with } \mathcal{M}(\omega, T) = \int_0^T d\tau e^{-i\omega\tau} \mathbf{m}(\tau). \quad (\text{S54})$$

This gives us the Equation (7) in the main text. In a special case, this result is greatly simplified when the velocity variation is a constant  $\delta v$  and thus  $\Omega(t)$  is also a constant denoted as  $\Omega$ . The error or infidelity can be reduced to

$$1 - \mathcal{F} = \frac{T \sin^2\theta}{4} \frac{S(0)}{2\hbar^2} + \frac{T \cos^2\theta}{4} \frac{S(\Omega) + S(-\Omega)}{4\hbar^2} = \frac{T}{4T_2}, \quad (\text{S55})$$

with  $1/T_2 = 1/T_\varphi + 1/(2T_1)$  where  $1/T_\varphi = \sin^2\theta S(0)/(2\hbar^2)$  and  $1/T_1 = [\cos^2\theta/(2\hbar^2)][S(\Omega) + S(-\Omega)]$ .

- 
- [1] S. K. Kim and O. Tchernyshyov, Mechanics of a ferromagnetic domain wall, *Journal of Physics: Condensed Matter* **35**, 134002 (2023).  
 [2] J. Zou, S. Bosco, B. Pal, S. S. P. Parkin, J. Klinovaja, and D. Loss, Quantum computing on magnetic racetracks with flying domain wall qubits, *Phys. Rev. Res.* **5**, 033166 (2023).